Electromagnetic Diffusion Model Canonical Example Suite Implementation Notes

Ian Flintoft[1]

Version 1.0, 24th February, 2018

Abstract *– These notes provide details of the implementation of the electromagnetic diffusion model for some canonical test cases using the finite element method with FreeFEM++. The treatment is terse and no attempt has been made to motivate the methods used or to provide comprehensive background and references. Results from the test-case implementations are compared to published measurement data.*

Contents

Abbreviations

ACS	(Average) Absorption Cross-Section
ADM	Acoustic Diffusion Model
AE	(Average) Absorption Efficiency
BC	Boundary Condition
COV	Coefficient of Variation
DDM	Dual Domain Model
DOF	Degrees of Freedom
EC	(Energy) Exchange Coefficient
EDM	Electromagnetic Diffusion Model
EEBC	Energy Exchange Boundary Condition
EM	Electromagnetic
FCBC	Flux Continuity Boundary Condition
FE	Finite Element
FEM	Finite Element Method
MFP	Mean-Free-Path
ODE	Ordinary Differential Equation
PDE	Partial Differential Equation
PDF	Probability Density Function
PWB	Power Balance
SDM	Single Domain Model
TCS	(Average) Transmission Cross-Section
TE	(Average) Transmission Efficiency

Symbols

Symbol	Unit	Variable	Definition
$w(\mathbf{r},t)$	$\mathrm{J\,m^{-3}}$	`w`	Average energy density in cavity
$D(\mathbf{r})$	$\mathrm{m^2\,s^{-1}}$	`D`	Diffusivity (Diffusion Coefficient)
Λ_V	$\mathrm{s^{-1}}$	`volLossRate`	Volumetric absorption loss rate
$p(\mathbf{r},t)$	$\mathrm{W\,m^{-3}}$	`volSrcDensity`	Volumetric power density source
c_0	$\mathrm{m\,s^{-1}}$	`c0`	Speed of light in free-space
λ	m	`MFP`	Mean free path
$\mathbf{J}(\mathbf{r},t)$	$\mathrm{W\,m^{-2}}$	`Jx, Jy, Jz`	Fickian energy density flux
V	$\mathrm{m^3}$	`cavityVolume`	Domain volume
S	$\mathrm{m^2}$	`cavityArea`	Domain surface area
κ	-	`specularity`	Empirical specular correction factor for diffusivity
$h(\mathbf{r})$	$\mathrm{m\,s^{-1}}$	`EC`	Energy exchange coefficient of domain boundary
$\alpha(\mathbf{r})$	-	`AE`	Average absorption efficiency of domain boundary
$\widehat{\mathbf{n}}$	-	-	Outward unit normal vector for domain
λ_{w}	m	`wallMFP`	Mean free path for wall scattering
D_{w}	$\mathrm{m^2\,s^{-1}}$	`wallD`	Diffusivity for wall scattering
$\alpha_{\mathrm{w}}(\mathbf{r})$		`wallAE`	Average absorption efficiency of walls
$h_{\mathrm{w}}(\mathbf{r})$	$\mathrm{m\,s^{-1}}$	`wallEC`	Energy exchange coefficient of walls
λ_{f}	m	`fittingMFP`	Mean free path for fitting scattering
D_{f}	$\mathrm{m^2\,s^{-1}}$	`fittingD`	Diffusivity for fitting scattering
$\alpha_{\mathrm{f}}(\mathbf{r})$	-	`fittingAE`	Average absorption efficiency of fittings
$\sigma_{\mathrm{f}}^{\mathrm{s}}$	$\mathrm{m^2}$	`fittingSCS`	Average scattering cross-section of fittings
$h_{\mathrm{f}}(\mathbf{r})$	$\mathrm{m\,s^{-1}}$	`fittingEC`	Energy exchange coefficient of fittings
n_V^{f}	$\mathrm{m^{-3}}$	`fittingConc`	Volumetric number density (concentration) of fittings
Λ_V^{f}	$\mathrm{s^{-1}}$	`fittingVolLossRate`	Volumetric absorption loss rate due to fittings
P^{t}	W	`srcTRP`	Source total (isotropic) radiated power
V_{s}	$\mathrm{m^3}$	`srcVolume`	Volumetric source volume
S_{s}	$\mathrm{m^2}$	`srcArea`	Surface source surface area
J_{s}	$\mathrm{W\,m^{-2}}$	`srcSurfaceExitance`	Surface source exitance
J_{c}	$\mathrm{W\,m^{-1}}$	`srcLineExitance`	Contour source line exitance
τ	-	`TE`	Average transmission efficiency of lossless aperture
$w_{\mathrm{r}}(\mathbf{r},t)$	$\mathrm{J\,m^{-3}}$	`wr`	Average reverberant energy density in cavity
$\mathbf{J}_{\mathrm{r}}(\mathbf{r},t)$	$\mathrm{W\,m^{-2}}$	`Jrx, Jyx, Jrz`	Reverberant energy density flux
$S(\mathbf{r},t)$	$\mathrm{W\,m^{-2}}$	`S`	Average scalar power density

1 Summary of the model

1.1 The diffusion equation

In the electromagnetic diffusion model (EDM) the diffuse electromagnetic energy density, $w(\mathbf{r}, t)$, at position $\mathbf{r}$ and time t in a closed domain Ω is assumed to satisfy the diffusion equation

$$\frac{\partial w(\mathbf{r},t)}{\partial t} - \boldsymbol{\nabla} \cdot [D(\mathbf{r}) \boldsymbol{\nabla} w(\mathbf{r},t)] + \Lambda_V w(\mathbf{r},t) = p(\mathbf{r},t) \quad \mathbf{r} \in \Omega \,, \tag{1.1}$$

where $D(\mathbf{r})$ is the potentially inhomogeneous diffusivity, Λ_V is an average volumetric absorption loss rate and $p(\mathbf{r}, t)$ is the volume power density of any sources (Picaut et al., 1999; Valeau et al., 2006; Navarro and Escolano, 2015; Savioja and Svensson, 2015). This is a second order parabolic partial differential equation (PDE). For time dependent problems the initial value of the energy density must be prescribed over the whole domain

$$w(\mathbf{r},t)|_{t_0} = w_0(\mathbf{r}) \quad \mathbf{r} \in \Omega \,. \tag{1.2}$$

The diffusivity accounts for the scattering within the cavity. To first approximation in a large sparsely populated domain it may be regarded as constant and is related to the mean-free-path (MFP) between scattering events, λ, by

$$D = \frac{1}{3} c_0 \lambda \,, \tag{1.3}$$

where c_0 is the speed of light in free-space.

The transport of average energy density is described by Fick's law for the energy density flux

$$\mathbf{J}(\mathbf{r},t) = -D(\mathbf{r}) \boldsymbol{\nabla} w(\mathbf{r},t). \tag{1.4}$$

The diffusion equation can therefore be interpreted as an equation of continuity

$$\frac{\partial w(\mathbf{r},t)}{\partial t} + \mathbf{J}(\mathbf{r},t) + \Lambda_V w(\mathbf{r},t) = p(\mathbf{r},t) \quad \mathbf{r} \in \Omega \tag{1.5}$$

for a flow of diffuse energy carried by pseudo-particles.

1.2 Scattering from the cavity walls

For an empty cavity without a strong aspect ratio (i.e. one that is approximately cubic) the MFP for scattering from the walls is given by (Navarro and Escolano, 2015)

$$\lambda_{\mathrm{w}} = \frac{4V}{S}, \tag{1.6}$$

where V and S are the interior volume and surface area of the cavity walls, which are given by

$$V = \iiint_\Omega \mathrm{d}V \tag{1.7}$$

$$S = \oiint_{\partial\Omega} \mathrm{d}S \,. \tag{1.8}$$

For cavities with one dimension much greater than the others the diffusivity becomes inhomogeneous, depending on the location of the source and the disposition of losses in the cavity (Visentin et al., 2012, 2015). For long cavities with relatively low loss a better estimate of the MFP may be given by

$$\lambda_{\mathrm{w}} = \sqrt{\frac{S}{4\pi}} \,; \tag{1.9}$$

however, this is a gross approximation which may be of limited scope and accuracy.

1.3 Scattering and absorption from fittings

If there are objects (fittings) in the cavity the overall MFP is the reciprocal of the sum of the reciprocals of the MFPs of the walls and fittings,

$$\frac{1}{\lambda} = \frac{1}{\lambda_{\rm w}} + \frac{1}{\lambda_{\rm f}}, \tag{1.10}$$

as is the corresponding overall diffusivity (Valeau et al., 2007)

$$\frac{1}{D} = \frac{1}{D_{\rm w}} + \frac{1}{D_{\rm f}}. \tag{1.11}$$

The diffusivity is therefore dominated by the shortest MFP. This behaviour of the diffusivity essentially derives from the additivity of the surface area of the fittings and walls. The MFP for scattering with identical fittings of surface area $S_{\rm f}$ and volumetric concentration $n_V^{\rm f} = N_{\rm f}/V$ can be estimated as (Valeau et al., 2007)

$$\lambda_{\rm f} = \frac{1}{\sigma_{\rm f}^{\rm s} n_V^{\rm f}} = \frac{4V}{S_{\rm f} N_{\rm f}}, \tag{1.12}$$

where $\sigma_{\rm f}^{s} = S_{\rm f}/4$ is the average scattering cross-section of the fittings. If the fittings are lossy then a term

$$\Lambda_V^{\rm f} = \frac{{\rm c}_0 \alpha_{\rm f}}{\lambda_{\rm f}} = {\rm c}_0 n_V^{\rm f} \sigma_{\rm f}^{\rm a} \tag{1.13}$$

must also be added to the volumetric scattering rate, Λ_V, that accounts for volumetric absorption processes. Here $\alpha_{\rm f}$ is the average absorption efficiency of the fittings and $\sigma_{\rm f}^{\rm a} = \alpha_{\rm f} S_{\rm f}/4$ their average absorption cross-section.

Attempts have also been made to include the effects of specular reflections by introducing an empirical "specularity factor", κ, into the diffusivity (Foy et al., 2009):

$$D \to \kappa D. \tag{1.14}$$

Empirically it is found that $1 \leq \kappa \lesssim 5$ and that κ depends on the scattering coefficient of the cavity walls, s, which is defined as the fraction of energy reflected diffusely ($0 \leq s \leq 1$). A simple empirical model was proposed in (Foy et al., 2009):

$$\kappa(s) = -2.238 \log_{\rm e}(s) + 1.549 \quad s \in [10^{-3}, 1], \tag{1.15}$$

though it was noted that the reverberation time was only accurate for $s > 0.4$. Further work by Navarro et al. (2013) suggests the acoustic diffusion model (ADM) for homogeneous single rooms only agrees to within $1\,{\rm dB}$ of ray tracing methods when $s > 0.6$ and $\alpha < 0.45$.

1.4 Absorption in the cavity walls

Absorption in the domain boundary is described by inhomogeneous Robin (also called Fourier or Type 3) boundary conditions

$$\widehat{\mathbf{n}} \cdot [D(\mathbf{r}) \boldsymbol{\nabla} w(\mathbf{r}, t)] + h(\mathbf{r}) w(\mathbf{r}, t) + J_{\rm in}(\mathbf{r}, t) - J_{\rm out}(\mathbf{r}, t) = 0 \quad \mathbf{r} \in \partial\Omega, \tag{1.16}$$

where $\widehat{\mathbf{n}}$ is the outward normal vector to the domain and $h(\mathbf{r})$ is an energy exchange coefficient (EC). $J_{\rm in}(\mathbf{r}, t)$ and $J_{\rm out}(\mathbf{r}, t)$ represent an in-flux and out-flux (exitance) of energy density to/from the surface respectively and can be used to model sources and energy exchange boundary conditions (EEBCs) as described below. Various models have been used in the acoustics literature to relate the exchange coefficient to the average absorption efficiency of the domain boundary, $\alpha(\mathbf{r})$ (Jing and Xiang, 2008; Xiang et al., 2009). The simplest is based on Sabine's estimate of the reverberation time (Sabine, 1922)

$$h(\mathbf{r}) = \tfrac{1}{4}{\rm c}_0 \alpha(r) \quad 0 \leq \alpha \lesssim 0.2 \tag{1.17}$$

and is regarded in acoustics as only accurate for low absorption $\alpha \lesssim 0.2$. A modified form

$$h(\mathbf{r}) = -c_0 \frac{\log_{10}(1 - \alpha(\mathbf{r}))}{4} \quad 0 \leq \alpha < 1 \tag{1.18}$$

based on the Eyring reverberation time has also been applied (Eyring, 1930). This empirically provides better results for moderate absorption, $\alpha \lesssim 0.5$, but becomes singular for $\alpha = 1$. More recently, a relation based on a radiative transport model has been proposed which appears to give good results over the full range of absorption efficiency (Jing and Xiang, 2008):

$$h(\mathbf{r}) = c_0 \frac{\alpha(\mathbf{r})}{2(2 - \alpha(\mathbf{r}))} \quad 0 \leq \alpha \leq 1. \tag{1.19}$$

The absorption efficiencies and exchange coefficients for the walls are denoted by $\alpha_\mathrm{w}(\mathbf{r})$ and $h_\mathrm{w}(\mathbf{r})$ respectively. Large fittings are more accurately modelled by including their surfaces as part of the domain boundary; in this case their absorption efficiencies and exchange coefficients are denoted by $\alpha_\mathrm{f}(\mathbf{r})$ and $h_\mathrm{f}(\mathbf{r})$ respectively and their losses are not included in the volumetric loss term.

1.5 Sources

A point source of instantaneous total radiated power (TRP) $P^\mathrm{t}(t)$ located at $\mathbf{r}_\mathrm{s}$ can be implemented as a volumetric power density

$$p(\mathbf{r}, t) = P^\mathrm{t}(t)\delta^{(3)}\left(\mathbf{r} - \mathbf{r}_\mathrm{s}\right). \tag{1.20}$$

The energy density near such a source contains a spurious direct term that can be subtract to give the reverberant energy density (Visentin et al., 2012); in 3D this correction is

$$w_\mathrm{r}(\mathbf{r}) = w(\mathbf{r}) - \frac{P^\mathrm{t}}{4\pi D \left|\mathbf{r} - \mathbf{r}_\mathrm{s}\right|} \tag{1.21}$$

while for 2D it is

$$w_\mathrm{r}(\mathbf{r}) = w(\mathbf{r}) - \frac{P^\mathrm{t}}{2\pi D} \log\left|\mathbf{r} - \mathbf{r}_\mathrm{s}\right|. \tag{1.22}$$

The true direct energy density is given by the inverse-square-law for the isotropic spreading of the power from the source:

$$w_\mathrm{d}(\mathbf{r}) = \frac{P^\mathrm{t}}{4\pi c_0 \left|\mathbf{r} - \mathbf{r}_\mathrm{s}\right|^2}. \tag{1.23}$$

The corresponding reverberant energy density flux is

$$\mathbf{J}_\mathrm{r}(\mathbf{r}, t) = -D\boldsymbol{\nabla}w_\mathrm{r}(\mathbf{r}) = \mathbf{J}(\mathbf{r}, t) - \frac{P^\mathrm{t}}{4\pi \left|\mathbf{r} - \mathbf{r}_\mathrm{s}\right|^3}\left(\mathbf{r} - \mathbf{r}_\mathrm{s}\right). \tag{1.24}$$

A uniform volumetric source over a sub-volume of the domain Ω_s can be implemented using

$$p(\mathbf{r}, t) = \frac{P^\mathrm{t}(t)}{V_s} \quad \mathbf{r} \in \Omega_\mathrm{s} \tag{1.25}$$

$$V_s = \iiint_{\Omega_\mathrm{s}} \mathrm{d}V. \tag{1.26}$$

The spurious direct energy density from such a source is reported to be less than for point sources (Visentin et al., 2012).

A portion of the domain boundary $\partial\Omega_\mathrm{s}$ can also be used as a surface source by introducing a source term into the Robin BC:

$$\widehat{\mathbf{n}}\cdot\left[D(\mathbf{r})\boldsymbol{\nabla}w(\mathbf{r}, t)\right] - J_\mathrm{s}(\mathbf{r}, t) = 0 \quad \mathbf{r} \in \partial\Omega_\mathrm{s}. \tag{1.27}$$

Here the exitance, $J_\mathrm{s}(\mathbf{r}, t)$, is

$$J_\mathrm{s}(\mathbf{r}, t) = \frac{P^\mathrm{t}(t)}{S_\mathrm{s}} \tag{1.28}$$

$$S_\mathrm{s} = \oiint_{\partial\Omega_\mathrm{s}} \mathrm{d}S. \tag{1.29}$$

1.6 Coupled domains

Consider the case of two cavities forming domains Ω_1 and Ω_2 with diffusivities $D_1(\mathbf{r})$ and $D_2(\mathbf{r})$ coupled by a translucent part of their shared boundary; the domain 1 side of the shared boundary is denoted by $\partial\Omega_{12}$ and the domain 2 side by $\partial\Omega_{21}$. If the coupling between the cavities is not too large we assume each cavity satisfies a diffusion equation with diffusivity given by the standard single cavity relationships above

$$\frac{\partial w_1(\mathbf{r},t)}{\partial t} - \boldsymbol{\nabla}\cdot[D_1(\mathbf{r})\boldsymbol{\nabla}w_1(\mathbf{r},t)] + \Lambda_{V;1}w_1(\mathbf{r},t) = p_1(\mathbf{r},t) \quad \mathbf{r}\in\Omega_1 \tag{1.30}$$

$$\frac{\partial w_2(\mathbf{r},t)}{\partial t} - \boldsymbol{\nabla}\cdot[D_2(\mathbf{r})\boldsymbol{\nabla}w_2(\mathbf{r},t)] + \Lambda_{V;2}w_2(\mathbf{r},t) = p_2(\mathbf{r},t) \quad \mathbf{r}\in\Omega_2 \tag{1.31}$$

and that on the non-shared parts of the walls normal Robin boundary conditions apply

$$\widehat{\mathbf{n}}_1\cdot[D_1(\mathbf{r})\boldsymbol{\nabla}w_1(\mathbf{r},t)] + h_1(\mathbf{r})w_1(\mathbf{r},t) = 0 \quad \mathbf{r}\in\partial\Omega_1/\partial\Omega_{12} \tag{1.32}$$

$$\widehat{\mathbf{n}}_2\cdot[D_2(\mathbf{r})\boldsymbol{\nabla}w_2(\mathbf{r},t)] + h_2(\mathbf{r})w_2(\mathbf{r},t) = 0 \quad \mathbf{r}\in\partial\Omega_2/\partial\Omega_{21}\,, \tag{1.33}$$

where $\widehat{n}_1$ and $\widehat{n}_2$ are outward normal vectors in their respective domains. On the shared wall an energy exchange boundary condition (EEBC) is applied ([Billon et al., 2008])

$$\widehat{\mathbf{n}}_1\cdot[D_1(\mathbf{r})\boldsymbol{\nabla}w_1(\mathbf{r},t)] + h_{11}(\mathbf{r})w_1(\mathbf{r},t) - h_{12}(\mathbf{r})w_2(\mathbf{r},t) = 0 \quad \mathbf{r}\in\partial\Omega_{12} \tag{1.34}$$

$$\widehat{\mathbf{n}}_2\cdot[D_2(\mathbf{r})\boldsymbol{\nabla}w_2(\mathbf{r},t)] + h_{22}(\mathbf{r})w_2(\mathbf{r},t) - h_{21}(\mathbf{r})w_1(\mathbf{r},t) = 0 \quad \mathbf{r}\in\partial\Omega_{21}\,, \tag{1.35}$$

where the exchange coefficients $h_{11}(\mathbf{r})$ and $h_{22}(\mathbf{r})$ describe the power lost on their respective sides of the boundary and $h_{12}(\mathbf{r})$ and $h_{21}(\mathbf{r})$ describe power coupled in from the other side.

If the coupling surface is a lossless reciprocal aperture with average transmission efficiency τ then

$$h_{12} = h_{21} = h_{22} = h_{11} = \frac{1}{4}c_0\tau \tag{1.36}$$

and

$$\widehat{\mathbf{n}}_1\cdot[D_1(\mathbf{r})\boldsymbol{\nabla}w_1(\mathbf{r},t)] + \tfrac{1}{4}c_0\tau\,[w_1(\mathbf{r},t) - w_2(\mathbf{r},t)] = 0 \quad \mathbf{r}\in\partial\Omega_{12} \tag{1.37}$$

$$\widehat{\mathbf{n}}_2\cdot[D_2(\mathbf{r})\boldsymbol{\nabla}w_2(\mathbf{r},t)] + \tfrac{1}{4}c_0\tau\,[w_2(\mathbf{r},t) - w_1(\mathbf{r},t)] = 0 \quad \mathbf{r}\in\partial\Omega_{21}\,. \tag{1.38}$$

In the geometric optics regime the energy lost through an aperture is indistinguishable from that absorbed in a perfect absorber of the same area; it can therefore be argued that the energy exchanged coefficient for an aperture should be given by

$$h_{ij}(\mathbf{r}) = c_0\frac{\tau}{2(2-\tau)} \quad 0 \le \tau \le 1 \tag{1.39}$$

in order to be consistent with the Jing and Xiang exchange coefficient for absorption ([1.19]).

Denoting the net energy flux from domain j into domain i by $J_{ij}(\mathbf{r},t)$ these boundary conditions can also be written

$$\widehat{\mathbf{n}}_1\cdot[D_1(\mathbf{r})\boldsymbol{\nabla}w_1(\mathbf{r},t)] - J_{12}(\mathbf{r},t) = 0 \quad \mathbf{r}\in\partial\Omega_{12} \tag{1.40}$$

$$\widehat{\mathbf{n}}_2\cdot[D_2(\mathbf{r})\boldsymbol{\nabla}w_2(\mathbf{r},t)] - J_{21}(\mathbf{r},t) = 0 \quad \mathbf{r}\in\partial\Omega_{21} \tag{1.41}$$

with

$$J_{12}(\mathbf{r},t) = -J_{21}(\mathbf{r},t) = \frac{1}{4}c_0\tau\,[w_2(\mathbf{r},t) - w_1(\mathbf{r},t)]\,. \tag{1.42}$$

Adding these and noting $\widehat{\mathbf{n}}_1 = -\widehat{\mathbf{n}}_2$ we find an energy density flux continuity boundary condition (FCBC) through the aperture ([Billon et al., 2008]):

$$\widehat{\mathbf{n}}_1\cdot[D_1(\mathbf{r})\boldsymbol{\nabla}w_1(\mathbf{r},t) - D_2(\mathbf{r})\boldsymbol{\nabla}w_2(\mathbf{r},t)] = 0 \quad \mathbf{r}\in\partial\Omega_{12}\,. \tag{1.43}$$

If there is dissipative loss associated with the aperture then

$$\widehat{\mathbf{n}}_1\cdot[D_1(\mathbf{r})\boldsymbol{\nabla}w_1(\mathbf{r},t)] - \widehat{\mathbf{n}}_2\cdot[D_2(\mathbf{r})\nabla w_2(\mathbf{r},t)] = \frac{1}{4}c_0\tau\,[w_2(\mathbf{r},t) - w_1(\mathbf{r},t)] + h_{22}(\mathbf{r})w_2(\mathbf{r},t) - h_{11}(\mathbf{r})w_1(\mathbf{r},t) \tag{1.44}$$

where $h_{11}, h_{22} > \frac{1}{4}c_0\tau$.

2 Kantorovich reduction to two dimensions

2.1 Separation and reduction to 2D

Systematic reduction from 3D to 2D can be made via the Kantorovich dimensional reduction approach for domains with a uniform cross-section in one direction, here taken to be the z-direction (Sequeira and Cortínez, 2012). This separates the energy density into

$$w(\mathbf{r}, t) = W(x, y, t)Z(z), \tag{2.1}$$

where the dimensionless function $Z(z)$ is assumed known a-priori (i.e. an anzatz), for example, here it is assumed to be quadratic. This function must satisfy the Robin BCs applied on the $z = 0$ and $z = L_z$ faces of the domain. If these upper and lower faces have the same uniform ECs, h_{w}, and the diffusivity in the domain is also uniform then

$$Z(z) = 1 + \xi \left(z - \frac{z^2}{L_z} \right), \tag{2.2}$$

where

$$\xi = \frac{h_{\mathrm{w}}}{D}. \tag{2.3}$$

Using the Kantorovich dimensional reduction approach shows that the energy density in the other two dimensions satisfies the 2D diffusion problem (Kantorovich and Krylov, 1964)

$$\begin{aligned}
\frac{\partial W(x,y,t)}{\partial t} \int_0^{L_z} Z(z)^2 \, \mathrm{d}z - D' \boldsymbol{\nabla}_{xy}^2 W(x, y, t) + (\Lambda_A' + \Lambda_Z') W(x, y, t) &= p'(x, y, t) & \mathbf{r} \in \Omega \\
D' \widehat{\mathbf{n}} \cdot \boldsymbol{\nabla}_{xy} W(x, y, t) + h'(x, y) W(x, y, t) &= 0 & \mathbf{r} \in \partial\Omega
\end{aligned} \tag{2.4}$$

where Ω is the cross-sectional area of the domain projected in the z-direction, $\partial\Omega$, is its perimeter and

$$D' = D \int_0^{L_z} Z(z)^2 \, \mathrm{d}z \tag{2.5}$$

$$\Lambda_Z' = -D \int_0^{L_z} \left(\frac{\mathrm{d}^2 Z(z)}{\mathrm{d}z^2} Z(z) \right) \mathrm{d}z \tag{2.6}$$

$$\Lambda_V' = \Lambda_V \int_0^{L_z} Z(z)^2 \, \mathrm{d}z \tag{2.7}$$

$$h'(x, y) = \int_0^{L_z} h(\mathbf{r}) Z(z)^2 \, \mathrm{d}z. \tag{2.8}$$

If the $z = 0$ and $z = L_z$ faces have the same uniform ECs then

$$\int_0^{L_z} Z(z) \, \mathrm{d}z = L_z + \xi \frac{L_z^2}{6} \tag{2.9}$$

$$\int_0^{L_z} Z(z)^2 \, \mathrm{d}z = L_z + \xi \frac{L_z^2}{3} + \xi^2 \frac{L_z^3}{30} \tag{2.10}$$

$$\int_0^{L_z} \left(Z(z) \frac{\mathrm{d}^2 Z(z)}{\mathrm{d}z^2} \right) \mathrm{d}z = -\xi \left(2 + \xi \frac{L_z}{3} \right). \tag{2.11}$$

3 Finite element solution

The diffusion equation can be solved numerical using a number of methods including the finite element method (FEM). In this section we outline the FEM solution and its implementation using FreeFEM++ (Hecht, 2013, 2017).

3.1 Weak form of the diffusion problem

To derive the weak formulation of the EDM we start from the PDE

$$\frac{\partial w(\mathbf{r},t)}{\partial t} - \boldsymbol{\nabla}\cdot[D(\mathbf{r})\boldsymbol{\nabla}w(\mathbf{r},t)] + \Lambda_V w(\mathbf{r},t) = p(\mathbf{r},t) \quad \mathbf{r}\in\Omega \tag{3.1}$$

and multiply throughout by a test function $u(\mathbf{r})$ and then integrate over the volume of the domain to give

$$\frac{\partial}{\partial t}\iiint_\Omega u(\mathbf{r})w(\mathbf{r},t)\,\mathrm{d}V - \iiint_\Omega u(\mathbf{r})\boldsymbol{\nabla}\cdot[D(\mathbf{r})\boldsymbol{\nabla}w(\mathbf{r},t)]\,\mathrm{d}V + \Lambda_V\iiint_\Omega u(\mathbf{r})w(\mathbf{r},t)\,\mathrm{d}V = \iiint_\Omega u(\mathbf{r})p(\mathbf{r},t)\,\mathrm{d}V. \tag{3.2}$$

Now assuming that all the functions are suitably smooth we apply the divergence theorem

$$\iiint_\Omega \boldsymbol{\nabla}\cdot\mathbf{F}(\mathbf{r})\,\mathrm{d}V = \oiint_{\partial\Omega}\mathbf{F}(\mathbf{r})\cdot\mathrm{d}\mathbf{S}\,. \tag{3.3}$$

First putting $\mathbf{F}(\mathbf{r}) = \varphi(\mathbf{r})\mathbf{G}(\mathbf{r})$ we obtain

$$\iiint_\Omega \varphi(\mathbf{r})\boldsymbol{\nabla}\cdot\mathbf{G}(\mathbf{r}) + \mathbf{G}(\mathbf{r})\cdot\boldsymbol{\nabla}\varphi(\mathbf{r})\,\mathrm{d}V = \oiint_{\partial\Omega}\varphi(\mathbf{r})\mathbf{G}(\mathbf{r})\cdot\mathrm{d}\mathbf{S} \tag{3.4}$$

and then letting $\mathbf{G}(\mathbf{r}) = \gamma(\mathbf{r})\boldsymbol{\nabla}\psi(\mathbf{r})$ gives

$$\iiint_\Omega \varphi(\mathbf{r})\boldsymbol{\nabla}\cdot[\gamma(\mathbf{r})\boldsymbol{\nabla}\psi(\mathbf{r})] + \gamma(\mathbf{r})\boldsymbol{\nabla}\psi(\mathbf{r})\cdot\boldsymbol{\nabla}\varphi(\mathbf{r})\,\mathrm{d}V = \oiint_{\partial\Omega}\varphi(\mathbf{r})\gamma(\mathbf{r})\boldsymbol{\nabla}\psi(\mathbf{r})\cdot\mathrm{d}\mathbf{S}\,. \tag{3.5}$$

Now letting $\varphi(\mathbf{r}) = u(\mathbf{r})$, $\gamma(\mathbf{r}) = D(\mathbf{r})$ and $\psi = w(\mathbf{r},t)$ we have

$$\iiint_\Omega u\boldsymbol{\nabla}\cdot[D\boldsymbol{\nabla}w]\,\mathrm{d}V = \oiint_{\partial\Omega}uD\boldsymbol{\nabla}w\cdot\mathrm{d}\mathbf{S} - \iiint_\Omega D\boldsymbol{\nabla}w\cdot\boldsymbol{\nabla}u\,\mathrm{d}V\,, \tag{3.6}$$

which can be used to reduce the second order derivative term in the integral form above to obtain

$$\frac{\partial}{\partial t}\iiint_\Omega u(\mathbf{r})w(\mathbf{r},t)\,\mathrm{d}V - \oiint_{\partial\Omega}u(\mathbf{r})D(\mathbf{r})\boldsymbol{\nabla}w(\mathbf{r},t)\cdot\mathrm{d}\mathbf{S} + \iiint_\Omega D(\mathbf{r})\boldsymbol{\nabla}w(\mathbf{r},t)\cdot\boldsymbol{\nabla}u(\mathbf{r})\,\mathrm{d}V$$
$$+ \Lambda_V\iiint_\Omega u(\mathbf{r})w(\mathbf{r},t)\,\mathrm{d}V = \iiint_\Omega u(\mathbf{r})p(\mathbf{r},t)\,\mathrm{d}V\,. \tag{3.7}$$

The most general form of the Robin BC

$$D(\mathbf{r})\widehat{\mathbf{n}}\cdot\boldsymbol{\nabla}w(\mathbf{r},t) + h(\mathbf{r})w(\mathbf{r},t) - J_\mathrm{s}(\mathbf{r},t) = 0 \tag{3.8}$$

is now inserted into the surface term to give the weak form of the diffusion problem:

$$\frac{\partial}{\partial t}\iiint_\Omega u(\mathbf{r})w(\mathbf{r},t)\,\mathrm{d}V + \iiint_\Omega D(\mathbf{r})\boldsymbol{\nabla}w(\mathbf{r},t)\cdot\boldsymbol{\nabla}u(\mathbf{r})\,\mathrm{d}V + \Lambda_V\iiint_\Omega u(\mathbf{r})w(\mathbf{r},t)\,\mathrm{d}V$$
$$+ \oiint_{\partial\Omega}u(\mathbf{r})h(\mathbf{r})w(\mathbf{r},t)\,\mathrm{d}S - \oiint_{\partial\Omega}u(\mathbf{r})J_\mathrm{s}(\mathbf{r},t)\,\mathrm{d}S - \iiint_\Omega u(\mathbf{r})p(\mathbf{r},t)\,\mathrm{d}V = 0\,. \tag{3.9}$$

This can be written more concisely as

$$\langle \dot{w}, u\rangle + a(w,u) - \langle J_\mathrm{s} + p, u\rangle = 0\,, \tag{3.10}$$

where $a(w,u)$ is the variational bilinear form

$$a(w,u) = \iiint_\Omega D(\mathbf{r})\boldsymbol{\nabla}w(\mathbf{r},t)\cdot\boldsymbol{\nabla}u(\mathbf{r})\,\mathrm{d}V + \Lambda_V\iiint_\Omega u(\mathbf{r})w(\mathbf{r},t)\,\mathrm{d}V + \oiint_{\partial\Omega}u(\mathbf{r})h(\mathbf{r})w(\mathbf{r},t)\,\mathrm{d}S \tag{3.11}$$

and the inner product is

$$\langle u, v\rangle = \iiint_\Omega u(\mathbf{r})v(\mathbf{r})\,\mathrm{d}V\,. \tag{3.12}$$

The above development is sufficient to implement a numerical solution of the EDM in FreeFEM++; for time-independent problems the essence of this implementation is:

```
problem EDM( w , u )
  = int3d(Omega)       ( D * ( dx(w) * dx(u) + dy(w) * dy(u) + dz(w) * dz(u) ) )
  + int3d(Omega)       ( w * v * LambdaV )
  + int2d(Omega,dOmega)( w * u * h )
  - int2d(Omega,dOmega)( u * Js )
  - int3d(Omega)       ( u * p );
```

If the diffusivity is inhomogeneous then D must be implemented using a suitably constructed FE space or using a macro, for example

```
func D = D1 * ( x <= partX ) + D2 * ( x > partX )
```

Similarly for the volume source term. For point sources an interpolated FE space can be used.

3.2 Discretisation and finite element spaces

The mesh is a discrete tessellation of the domain

$$\Omega \approx \Omega_h = \bigcup_{k=1}^{n_{\mathrm{T}}} T_k \tag{3.13}$$

using n_{T} elements T_k with characteristics dimension h:

$$T_h = \{T_k : k = 1, \ldots, n_{\mathrm{T}}\} . \tag{3.14}$$

The elements are typically triangles in 2D or tetrahedra in 3D. The maximum edge size in the mesh for an accurate approximate solution is determined by the MFP in the EDM: $h \lesssim \lambda/10$. The number of vertices in the mesh is denoted by n_{v} and the boundary of the discrete domain is denoted by $\partial\Omega \approx \partial\Omega_h$. The finite element space on T_h, is denoted by $V_h(T_h, X)$:

$$V_h(T_h, X) = \left\{ w(\mathbf{r}) : w(\mathbf{r}) = \sum_{k=1}^{M} w_k \phi_k(\mathbf{r}), \ w_k \in \mathbb{R} \right\}, \tag{3.15}$$

where X denotes the types of finite elements. For example, piecewise continuous elements are denoted by P_1. M is the dimension of V_h, i.e. the total number of vertices, which is the number of elements times the number of matching points on each element. w_k are termed the degrees of freedom of w and M is the number of degrees of freedom (DOF). The basis functions $\phi_k(\mathbf{r})$ are usually defined in terms of barycentric coordinates. For a point $\mathbf{r} \in T_k$ the barycentric coordinates $\lambda_i^k(\mathbf{r})$ are

$$\mathbf{r} = \sum_{i=1}^{n_{\mathrm{m}}} \lambda_i^k \mathbf{r}_i \tag{3.16}$$

with

$$\sum_{i=1}^{n_{\mathrm{m}}} \lambda_i^k = 1 ,$$

where $\mathbf{r}_i$ are the n_{m} vertices of T_k. The restriction of ϕ_i on T_k is then λ_i^k.

Now using the Galerkin method we approximate both the energy density and test function using the same FE space

$$w(\mathbf{r}, t) \approx w_h(\mathbf{r}, t) = \sum_{j=1}^{M} w_j(t) \phi_j(\mathbf{r}) \tag{3.17}$$

$$u(\mathbf{r}) \approx u_h(\mathbf{r}) = \sum_{i=1}^{M} u_i \phi_i(\mathbf{r}) \tag{3.18}$$

and substitute these into the weak form to obtain

$$\sum_{i=1}^{M}\sum_{j=1}^{M} u_i \dot{w}_j \iiint_\Omega \phi_i(\mathbf{r})\phi_j(\mathbf{r})\,\mathrm{d}V + \sum_{i=1}^{M}\sum_{j=1}^{M} u_i w_j \iiint_\Omega D(\mathbf{r})\boldsymbol{\nabla}\phi_i(\mathbf{r})\cdot\boldsymbol{\nabla}\phi_j(\mathbf{r})\,\mathrm{d}V$$

$$+ \Lambda_V \sum_{i=1}^{M}\sum_{j=1}^{M} u_i w_j \iiint_\Omega \phi_i(\mathbf{r})\phi_j(\mathbf{r})\,\mathrm{d}V + \sum_{i=1}^{M}\sum_{j=1}^{M} u_i w_j \oiint_{\partial\Omega} h(\mathbf{r})\phi_i(\mathbf{r})\phi_j(\mathbf{r})\,\mathrm{d}S$$

$$- \sum_{i=1}^{M} u_i \oiint_{\partial\Omega} \phi_i(\mathbf{r})J_{\mathrm{s}}(\mathbf{r},t)\,\mathrm{d}S - \sum_{i=1}^{M} u_i \iiint_\Omega \phi_i(\mathbf{r})p(\mathbf{r},t)\,\mathrm{d}V = 0\,. \tag{3.19}$$

Denoting the discrete matrix operators by

$$D_{ij} = \iiint_\Omega D(\mathbf{r})\boldsymbol{\nabla}\phi_i(\mathbf{r})\cdot\boldsymbol{\nabla}\phi_j(\mathbf{r})\,\mathrm{d}V \tag{3.20}$$

$$M_{ij} = \iiint_\Omega \phi_i(\mathbf{r})\phi_j(\mathbf{r})\,\mathrm{d}V \tag{3.21}$$

$$H_{ij} = \oiint_{\partial\Omega} \phi_j(\mathbf{r})h(\mathbf{r})\phi_i(\mathbf{r})\,\mathrm{d}S \tag{3.22}$$

$$J_i^{\mathrm{s}}(t) = \oiint_{\partial\Omega} \phi_i(\mathbf{r})J_{\mathrm{s}}(\mathbf{r},t)\,\mathrm{d}S \tag{3.23}$$

$$P_i(t) = \iiint_\Omega \phi_i(\mathbf{r})p(\mathbf{r},t)\,\mathrm{d}V \tag{3.24}$$

this can be written as

$$\sum_{i=1}^{M}\sum_{j=1}^{M} u_i M_{ij} \dot{w}_j + \sum_{i=1}^{M}\sum_{j=1}^{M} u_i D_{ij} w_j + \Lambda_V \sum_{i=1}^{M}\sum_{j=1}^{M} u_i M_{ij} w_j + \sum_{i=1}^{M}\sum_{j=1}^{M} u_i H_{ij} w_j$$

$$- \sum_{i=1}^{M}\sum_{j=1}^{M} u_i J_i^{\mathrm{s}} - \sum_{i=1}^{M} u_i P_i = 0\,. \tag{3.25}$$

D_{ij} is the stiffness matrix, M_{ij} is the mass matrix and $\Lambda_V M_{ij} + H_{ij}$ is a dissipation matrix. This can be written in matrix form as

$$\mathbf{u}^{\mathsf{T}} M \dot{\mathbf{w}} + \mathbf{u}^{\mathsf{T}} D \mathbf{w} + \Lambda_V \mathbf{u}^{\mathsf{T}} M \mathbf{w} + \mathbf{u}^{\mathsf{T}} H \mathbf{w} - \mathbf{u}^{\mathsf{T}} \mathbf{J}^{\mathrm{s}} - \mathbf{u}^{\mathsf{T}} \mathbf{P} = 0\,, \tag{3.26}$$

where $\mathbf{u}$ and $\mathbf{w}$ are column vectors containing the DOFs and T denotes the transpose. Since the system is linear it can be solved by testing with each basis function separately and so it is equivalent to the linear system of ordinary differential equations (ODEs)

$$M \dot{\mathbf{w}} + D \mathbf{w} + \Lambda_V M \mathbf{w} + H \mathbf{w} - \mathbf{J}^{\mathrm{s}} - \mathbf{P} = \mathbf{0}\,. \tag{3.27}$$

This reduces to a linear algebraic system

$$(D + \Lambda_V M + H)\,\mathbf{w} - (\mathbf{J}^{\mathrm{s}} + \mathbf{P}) = \mathbf{0} \tag{3.28}$$

for time-independent problems.

Time dependent systems can be solved by applying a finite difference scheme to the time derivative. Sampling $w(\mathbf{r},t) = w(\mathbf{r},\Delta t) = w^n(\mathbf{r})$ and applying a Euler backward difference approximation the time derivative term is

$$\langle \dot{w}, u \rangle \approx \left\langle \frac{w^n - w^{n-1}}{\Delta t}, u \right\rangle = \iiint_\Omega u(\mathbf{r}) \frac{w^n(\mathbf{r}) - w^{n-1}(\mathbf{r})}{\Delta t}\,\mathrm{d}V\,. \tag{3.29}$$

The weak variational problem

$$\left\langle \frac{w^n - w^{n-1}}{\Delta t}, u \right\rangle + a(w, u) - \langle J_{\mathrm{s}} + p, u \rangle = 0, \tag{3.30}$$

can then be solved implicitly for the solution $w^n(\mathbf{r})$ at time step n using the known solution $w^{n-1}(\mathbf{r})$ at the previous time-step. This leads to the FreeFEM++ time-stepping implementation:

```
    real dt = meshSize * meshSize / 2 / D;
    Vh w , wold = wpwb , u;

    problem EDM( w , u )
     = int3d(Omega)        ( w / dt * u )
     - int3d(Omega)        ( wold / dt * u )
     + int3d(Omega)        ( D * ( dx(w) * dx(u) + dy(w) * dy(u) + dz(w) * dz(u) ) ) )
     + int3d(Omega)        ( w * v * LambdaV )
     + int2d(Omega,dOmega)( w * u * h )
     - int2d(Omega,dOmega)( u * Js )
     - int3d(Omega)        ( u * p );

    for( real t = 0 ; t < maxTime ; t += dt ) {
      wold = w;
      EDM;
    }
```

This implicit scheme is unconditionally stable and so the stability criterion $\Delta t \leq h^2/2D$, where h is the smallest edge length in the mesh, that applies to explicit finite-difference approximations of the diffusion equations does not have to be satisfied. A large time-step still has an impact on the accuracy of the solution. It appears that a value of $\Delta t \lesssim \Delta t_{\text{ref}}/10$, where $\Delta t_{\text{ref}} = L_x^2/2D$ is the characteristic diffusion time across the cavity gives a reasonable trade-off between accuracy and computation time for the cases studied here.

3.3   Iterative methods for coupled domains

For the case of two domains coupled through an EEBC the weak forms in each domain are

$$
\frac{\partial}{\partial t} \iiint_{\Omega_1} u_1(\mathbf{r}) w_1(\mathbf{r},t) \, \mathrm{d}V + \iiint_{\Omega_1} D_1(\mathbf{r}) \boldsymbol{\nabla} w_1(\mathbf{r},t) \cdot \boldsymbol{\nabla} u_1(\mathbf{r}) \, \mathrm{d}V + \Lambda_{V;1} \iiint_{\Omega_1} u_1(\mathbf{r}) w_1(\mathbf{r},t) \, \mathrm{d}V
$$
$$
+ \oiint_{\partial\Omega_1/\partial\Omega_{12}} u_1(\mathbf{r}) h_1(\mathbf{r}) w_1(\mathbf{r},t) \, \mathrm{d}S - \oiint_{\partial\Omega_1/\partial\Omega_{12}} u_1(\mathbf{r}) J_{\mathrm{s};1}(\mathbf{r},t) \, \mathrm{d}S + \oiint_{\partial\Omega_{12}} u_1(\mathbf{r}) h_{11}(\mathbf{r}) w_1(\mathbf{r},t) \, \mathrm{d}S
$$
$$
- \oiint_{\partial\Omega_{12}} u_1(\mathbf{r}) J_{12}(\mathbf{r},t) \, \mathrm{d}S - \iiint_{\Omega_1} u_1(\mathbf{r}) p_1(\mathbf{r},t) \, \mathrm{d}V = 0 \tag{3.31}
$$

and

$$
\frac{\partial}{\partial t} \iiint_{\Omega_2} u_2(\mathbf{r}) w_2(\mathbf{r},t) \, \mathrm{d}V + \iiint_{\Omega_2} D_2(\mathbf{r}) \boldsymbol{\nabla} w_2(\mathbf{r},t) \cdot \boldsymbol{\nabla} u_2(\mathbf{r}) \, \mathrm{d}V + \Lambda_{V;2} \iiint_{\Omega_2} u_2(\mathbf{r}) w_2(\mathbf{r},t) \, \mathrm{d}V
$$
$$
+ \oiint_{\partial\Omega_2/\partial\Omega_{21}} u_2(\mathbf{r}) h_2(\mathbf{r}) w_2(\mathbf{r},t) \, \mathrm{d}S - \oiint_{\partial\Omega_2/\partial\Omega_{21}} u_2(\mathbf{r}) J_{\mathrm{s};2}(\mathbf{r},t) \, \mathrm{d}S + \oiint_{\partial\Omega_{21}} u_2(\mathbf{r}) h_{22}(\mathbf{r}) w_2(\mathbf{r},t) \, \mathrm{d}S
$$
$$
- \oiint_{\partial\Omega_{21}} u_2(\mathbf{r}) J_{21}(\mathbf{r},t) \, \mathrm{d}S - \iiint_{\Omega_2} u_2(\mathbf{r}) p_2(\mathbf{r},t) \, \mathrm{d}V = 0 \, , \tag{3.32}
$$

where the energy density fluxes coupled between the cavities are

$$
J_{12}(\mathbf{r},t) = h_{12}(\mathbf{r}) w_2(\mathbf{r},t) \quad \mathbf{r} \in \partial\Omega_{12} \tag{3.33}
$$

$$
J_{21}(\mathbf{r},t) = h_{21}(\mathbf{r}) w_1(\mathbf{r},t) \quad \mathbf{r} \in \partial\Omega_{21} \, . \tag{3.34}
$$

The system can be solved using a Robin-Robin iterative algorithm (Discacciati et al., 2007). We first initialise $J_{12}(\mathbf{r},t)$ using the homogeneous power balance (PWB) solution, $w_{2;\mathrm{h}}$, in Ω_2

$$
J_{12}(\mathbf{r},t) = h_{12}(\mathbf{r}) w_{2;\mathrm{h}} \quad \mathbf{r} \in \partial\Omega_{12} \tag{3.35}
$$

and then solve the FE system (3.31) in domain Ω_1 using this value to give $w_1(\mathbf{r}, t)$. $J_{21}(\mathbf{r}, t)$ can then be calculated from (3.34), and hence the FE system (3.32) in domain Ω_2 can be solved for $w_2(\mathbf{r}, t)$. This process is repeated until the solution has converged; this typically only requires a handful of iterations. The complete iteration algorithm is:

$$\text{Initialise} : J_{12}(\mathbf{r}, t) = h_{12}(\mathbf{r})w_{2;\mathrm{h}}$$
$$(*)\,\text{Solve for } w_1 : \langle w_1, u_1 \rangle + a(w_1, u_1) - \langle u_1, J_{12} \rangle - \langle u_1, p_1 \rangle = 0$$
$$\text{Update} : J_{21}(\mathbf{r}, t) = h_{21}(\mathbf{r})w_1$$
$$\text{Solve for } w_2 : \langle w_2, u_2 \rangle + a(w_2, u_2) - \langle u_2, J_{21} \rangle - \langle u_2, p_1 \rangle = 0$$
$$\text{Update} : J_{12}(\mathbf{r}, t) = h_{12}(\mathbf{r})w_2$$
$$\text{Repeat} : \text{from } (*)$$

For a FCBC

$$\widehat{\mathbf{n}}_1 \cdot [D_1(\mathbf{r})\boldsymbol{\nabla} w_1(\mathbf{r}, t) - D_2(\mathbf{r})\boldsymbol{\nabla} w_2(\mathbf{r}, t)] = 0 \tag{3.36}$$

an iterative scheme can be also be applied. The weak forms are as in (3.31) and (3.32), but with the $h_{11}(\mathbf{r})$ and $h_{22}(\mathbf{r})$ terms omitted - the corresponding bilinear terms are denoted by $\tilde{a}(w_1, u_1)$ and $\tilde{a}(w_2, u_2)$ respectively. Robin BCs are enforced on each side of the boundary

$$\widehat{\mathbf{n}}_1 \cdot D_1(\mathbf{r})\boldsymbol{\nabla} w_1(\mathbf{r}, t) + J_{21}(\mathbf{r}, t) = 0 \tag{3.37}$$
$$\widehat{\mathbf{n}}_2 \cdot D_2(\mathbf{r})\boldsymbol{\nabla} w_2(\mathbf{r}, t) - J_{21}(\mathbf{r}, t) = 0 \tag{3.38}$$

in terms of the net energy flux J_{21} from domain 1 into domain 2. At each iteration this can be updated using a relaxation scheme with relaxation parameter $\beta \sim 0.1$:

$$\text{Initialise} : J_{12}(\mathbf{r}, t) = J_{21}(\mathbf{r}, t) = 0$$
$$(*)\,\text{Solve for } w_1 : \langle w_1, u_1 \rangle + \tilde{a}(w_1, u_1) - \langle u_1, J_{12} \rangle - \langle u_1, p_1 \rangle = 0$$
$$\text{Solve for } w_2 : \langle w_2, u_2 \rangle + \tilde{a}(w_2, u_2) - \langle u_2, J_{21} \rangle - \langle u_2, p_1 \rangle = 0$$
$$\text{Update} : J_{21}(\mathbf{r}, t) = \beta J_{21}(\mathbf{r}, t) + (1 - \beta)h_{21}(\mathbf{r})\,[w_1(\mathbf{r}, t) - w_2(\mathbf{r}, t)]$$
$$\text{Update} : J_{12}(\mathbf{r}, t) = \beta J_{12}(\mathbf{r}, t) + (1 - \beta)h_{12}(\mathbf{r})\,[w_2(\mathbf{r}, t) - w_1(\mathbf{r}, t)]$$
$$\text{Repeat} : \text{from } (*)$$

As described in Section 1.6 the EEBC and FCBC are equivalent in the case of a lossless aperture.

Continuity of both the energy density and its flux can be enforced using a non-overlapping Schwarz domain decomposition method (Lions, 1990). The weak forms are the same as for the FCBC method; however, the net flux is updated using

$$\text{Initialise} : J_{12}(\mathbf{r}, t) = J_{21}(\mathbf{r}, t) = 0$$
$$(*)\,\text{Solve for } w_1 : \langle w_1, u_1 \rangle + \tilde{a}(w_1, u_1) - \langle u_1, J_{12} \rangle - \langle u_1, p_1 \rangle = 0$$
$$\text{Solve for } w_2 : \langle w_2, u_2 \rangle + \tilde{a}(w_2, u_2) - \langle u_2, J_{21} \rangle - \langle u_2, p_1 \rangle = 0$$
$$\text{Update} : J_{21}(\mathbf{r}, t) = J_{21}(\mathbf{r}, t) + \beta h_{21}(\mathbf{r})\,[w_1(\mathbf{r}, t) - w_2(\mathbf{r}, t)]$$
$$\text{Update} : J_{12}(\mathbf{r}, t) = -J_{21}(\mathbf{r}, t)$$
$$\text{Repeat} : \text{from } (*)$$

where the sign and magnitude of β are chosen to give a stable scheme. This Schwarz approach is equivalent to using a single domain method. Convergence is typically slower than for the EEBC and FCBC schemes above.

3.4 Two dimensional FEM solution

The weak form of the reduced 2D problem is

$$
\int_0^{L_z} Z(z)^2 \, \mathrm{d}z \iint_\Omega U \frac{\partial W}{\partial t} \, \mathrm{d}x \, \mathrm{d}y + D' \iint_\Omega \frac{\partial W}{\partial x} \frac{\partial U}{\partial x} + \frac{\partial W}{\partial y} \frac{\partial U}{\partial y} \, \mathrm{d}x \, \mathrm{d}y
$$
$$
+ \left(\Lambda_V' + \Lambda_Z' \right) \iint_\Omega UW \, \mathrm{d}x \, \mathrm{d}y + \oint_{\partial\Omega} U h' \left(x, y \right) W \, \mathrm{d}l
$$
$$
- \oint_{\partial\Omega} U J_c' \left(x, y \right) W \, \mathrm{d}l - \iint_\Omega U p_s' \left(x, y \right) \, \mathrm{d}x \, \mathrm{d}y = 0 \,, \tag{3.39}
$$

where

$$
p_s' \left(x, y \right) = \int_0^{L_z} Z(z) p \left(x, y, z, t \right) \, \mathrm{d}z \,. \tag{3.40}
$$

Note that this implicitly replaces the point source by a line source with the same TRP, which will cause errors in the vicinity of the source; these errors will increase with increasing loss in the cavity.

For time-independent problems the 2D FreeFEM++ implementation is

```
problem EDM( W , U )
 = int2d(Omega)      ( D * ( dx(W) * dx(U) + dy(W) * dy(U) ) )
 + int2d(Omega)      ( W * V * ( LambdaV + LambdaZ ) )
 + int1d(Omega,dOmega)( W * U * h )
 - int1d(Omega,dOmega)( U * Jc )
 - int2d(Omega)      ( U * ps );
```

4 Canonical test cases

4.1 Test case specifications

The canonical test cases are based on the geometry of a cuboid cavity occupying the volume $0 \leq x \leq L_x$, $0 \leq y \leq L_y$ and $0 \leq z \leq L_z$ shown in Figure 1. The walls are assumed to have a homogeneous absorption efficiency of α_{wall} and the cavity is excited by an isotropic source of total radiated power $P_{\mathrm{src}}^{\mathrm{t}}$ located at $(x_{\mathrm{src}}, y_{\mathrm{src}}, L_z/2)$. An absorbing cylinder of radius a_{cyl} and height L_z can be positioned in the cavity, orientated with its axis in the z-direction, centred at $(x_{\mathrm{cyl}}, y_{\mathrm{cyl}}, L_z/2)$. The cylinder is assumed to have a homogeneous absorption efficiency of α_{cyl}.

The cavity can also be partitioned into two sub-cavities leaving a hole of width w_{hole} with the full height of the cavity located in the region $L_y - w_{\mathrm{hole}} \leq y \leq L_y$, $0 \leq z \leq L_z$ of the shared $x = x_{\mathrm{part}}$ wall. The hole was chosen to span the whole cavity so that the dimensional reduction technique is applicable and it was located along the edge of the partition for experimental convenience in the validation measurements. The thickness of the partition is denoted t_{part}.

The values of the parameters are given in Table 1. The wall and cylinder absorption efficiencies were chosen to match those of the physical cavity and cylinder used for the validation measurements described in (Flintoft et al., 2017). Note that the cylinder centre's x-coordinate is slightly different in the unpartitioned and partitioned cavities in order to be consistent with measurement data.

4.2 Single and dual domain models

The EDM of an unpartitioned cavity can be simply implemented using a single domain model (SDM) as shown in Figure 2(a). The diffusivity D of the domain Ω is uniform and the surfaces forming the walls, $\partial\Omega^{\mathrm{wall}}$, cylinder, $\partial\Omega^{\mathrm{cyl}}$, and possibly the source, $\partial\Omega^{\mathrm{src}}$, are identified. The surface bounding the source is used if the source is implemented as a surface or volume source, but is not used for a point source.

For coupled cavities there are a number of ways to implement the EDM. The sub-cavities can be modelled as a single contiguous domain with the aperture between them explicitly represented in the geometry; this is again an SDM and is illustrated in Figure 2(b). The surfaces of the walls in each sub-cavity, $\partial\Omega_1^{\mathrm{wall}}$ and $\partial\Omega_2^{\mathrm{wall}}$ are identified and it is convenient to also explicitly identify the portions of
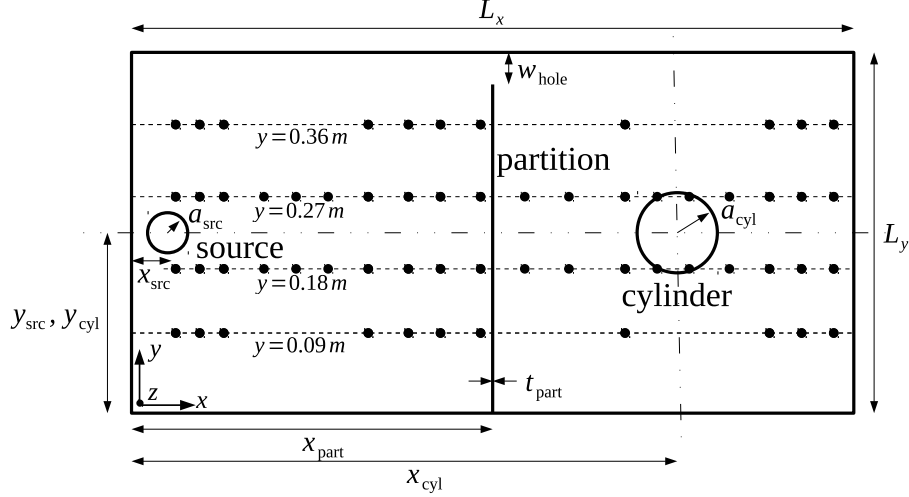
Figure 1: Cross-section in the xy-plane of the test case geometry. The small black dots represent the probe locations in the z=h plane used for the measurements.

the partition surface which face into each sub-cavity, $\partial\Omega_1^{\text{part}}$ and $\partial\Omega_2^{\text{part}}$. While only a single domain is modelled an inhomogeneous diffusivity is used to assign the appropriate diffusivities D_1 and D_2 in each sub-cavity:

$$D(\mathbf{r}) = \begin{cases} D_1 & x <= x_{\text{part}} \\ D_2 & x > x_{\text{part}} \end{cases} . \tag{4.1}$$

The energy density through the hole in this case satisfies the natural continuity boundary conditions for its value and derivative.

Alternatively the partitioned cavity can be implemented as a dual domain model (DDM) as shown in Figure 3, in which the sub-cavities are represented as completely separate domains Ω_1 and Ω_2. The surface corresponding to the hole is meshed as part of the surface bounding each sub-cavity and identified as $\partial\Omega_{12}^{\text{hole}}$ and $\partial\Omega_{21}^{\text{hole}}$ in the source and coupled sub-cavities respectively. The diffusivity in each sub-cavity is homogeneous with values D_1 and D_2 respectively. A appropriate boundary condition must be applied on the surfaces $\partial\Omega_{12}^{\text{hole}}$ and $\partial\Omega_{21}^{\text{hole}}$:

- **EEBC**: Exchange coefficients are used to enforce Robin BCs according to (1.34)-(1.35).

- **FCBC**: The energy density flux is forced to be continuous through the hole using (1.43). For lossless apertures with unity transmission efficiency this is equivalent to the EEBC;

- **Schwarz**: A non-overlapping Schwarz algorithm can be applied which enforces continuity of both the energy density and its flux; this is equivalent to using an SDM;

The SDM/Schwarz approach implicitly assumes that the aperture is electrical large and may only be accurate in this regime. The EEBC/FCBC method allow discontinuity of the energy density across aperture, which may be more appropriate for apertures which are in the resonant regime. For electrically small apertures the EEBC approach must be used and the appropriate transmission efficiency (TE) included. These conjectures on the realm of validity of the different aperture modelling approaches require verification, either by experiment or using full-wave simulation.

4.3 Overall solution work-flow

The overall solution of the EDM is implemented using a combination of Open Source tools:

1. **Gmsh**: For 3D solutions a parametric CAD model of the geometry is created using Gmsh (Geuzaine and Remacle, 2009). Gmsh is then used to created a tetrahedral mesh from this CAD model, which

Parameter	Variable	Value
Geometrical		
L_x	`Lx`	$0.90\,\text{m}$
L_y	`Ly`	$0.45\,\text{m}$
L_z	`Lz`	$0.45\,\text{m}$
x_{part}	`partX`	$0.45\,\text{m}$
t_{part}	`partThickness`	$0.005\,\text{m}$
w_{hole}	`holeWidth`	$0.04\,\text{m}$
x_{src}	`srcX`	$0.05\,\text{m}$
y_{src}	`srcY`	$0.225\,\text{m}$
z_{src}	`srcZ`	$0.225\,\text{m}$
a_{src}	`srcRadius`	$0.02\,\text{m}$
x_{cyl}	`cylX`	$0.675/0.700\,\text{m}^{\text{a}}$
y_{cyl}	`cylY`	$0.225\,\text{m}$
z_{cyl}	`cylZ`	$0.225\,\text{m}$
a_{cyl}	`cylRadius`	$0.05\,\text{m}$
Electromagnetic		
$P_{\text{src}}^{\text{t}}$	`srcTRP`	$1\,\text{W}$
α_{wall}	`wallAE`	0.0027
α_{part}	`partAE`	0.0027
α_{cyl}	`cylAE`	0.95

Table 1: Primary parameters and variable names for the test cases. [a]`cylX` is 0.7 in the unpartitioned cavity and 0.675 m in the partitioned cavity.

is then exported using the INRIA Medit format. As an example, the mesh for the loaded partitioned cavity is shown in Figure 4.

2. **FreeFEM++**: The FEM solution is determined using FreeFEM++ (Hecht, 2013). For 2D solutions the mesh is created directly within FreeFEM++, while for 3D solutions the mesh is imported in INRIA Medit format. The resulting energy density and energy density flux are exported in sampled form to ASCII files.

3. **Octave**: Post-processing is carried out by importing the sampled energy density and energy density flux into GNU Octave. The post-processing scripts are compatible with MATLAB.

The input for Gmsh, FreeFEM++ and Octave is all taken from the same ASCII text file `parameters.geo`, which is in Gmsh's "geo" format. The file contains a series of lines, each of which assigns a value to a variable:

```
isSrc = 0;             // Whether to mesh the source as a spherical surface [0/1].
isCyl = 1;             // Whether to include the cylinder [0/1].
isPart = 1;            // Whether to include the partition [0/1].
isSabine = 1;          // Whether to use Sabine or Jing & Xiang absorption factor model [0/1].
Lx = 0.9;              // Cavity size in x-direction [m].
Ly = 0.45;             // Cavity size in y-direction [m].
Lz = 0.45;             // Cavity size in z-direction [m].
wallAE = 0.0027;       // Absorption efficiency of walls [-].
partX = 0.45;          // x-coordinate of partition [m].
partThickness = 0.005; // Partition thickness [m].
```
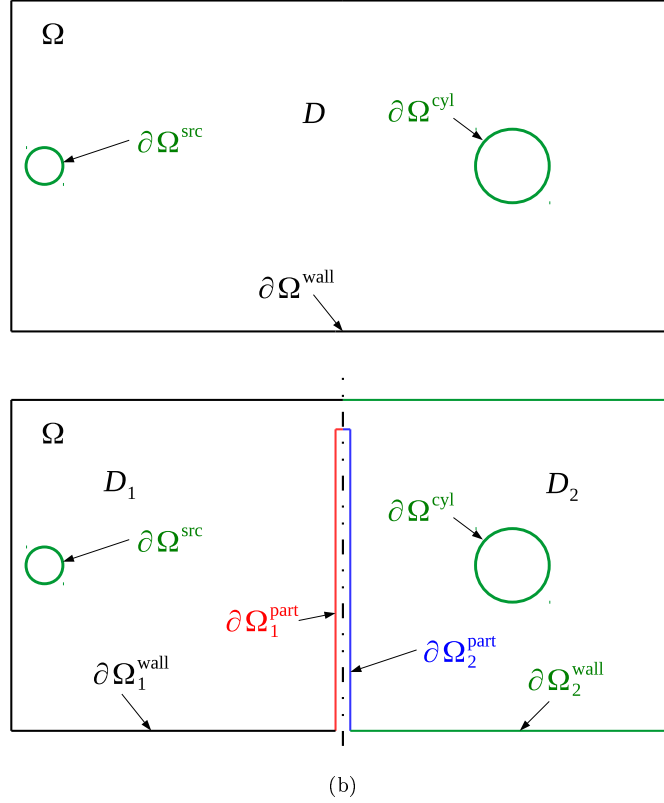
Figure 2: Domain nomenclature for the single domain model (SDM) implementation of the single cavity (a) and partitioned cavity (b).

```
partAE = 0.0027;         // Absorption efficiency of partition [-].
holeWidth = 0.04;        // Aperture width [m].
holeTE = 1.0;            // transmission efficiency of hole [-].
cylXWithPart = 0.675;    // x-coordinate of cylinder if partition is present [m].
cylXWithoutPart = 0.7;   // x-coordinate of cylinder if partition is not present [m].
cylY = 0.225;            // y-coordinate of cylinder [m].
cylRadius = 0.05;        // Cylinder radius [m].
cylAE = 0.95;            // Absorption efficiency of cylinder [-].
srcX = 0.05;             // x-coordinates of source [m].
srcY = 0.225;            // y-coordinates of source [m].
srcZ = 0.225;            // z-coordinates of source [m].
srcRadius = 0.02;        // Source radius if meshed as sphere [m].
srcTRP = 1;              // Total radiated power of source [W].
```

In order for FreeFEM++ and Octave to be able to parse the file correctly it is essential that spaces are left on either side of the "=" sign. The order of the parameters is not significant.

In addition to the geometrical and electromagnetic parameters defined in Table 1 four boolean parameters isSrc, isCyl, isPart and isSabine are also used:

- isSrc: If true, a small sphere is added to the mesh to represent the source using a surface, otherwise an interpolated delta function source is applied;

- isCyl: If true, the cylinder is included in the geometry;

- isPart: If true, the partition is included;

- isSabine: If true, the Sabine EC (1.17) is used, otherwise the Jing and Xiang EC (1.19) is used.
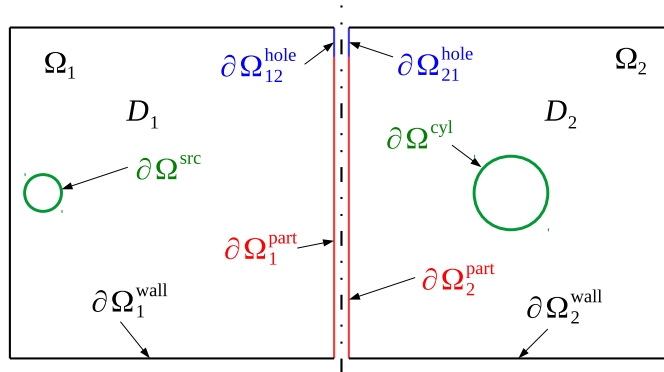
Figure 3: Domain nomenclature for the dual domain model (DDM) implementation of the partitioned cavity.
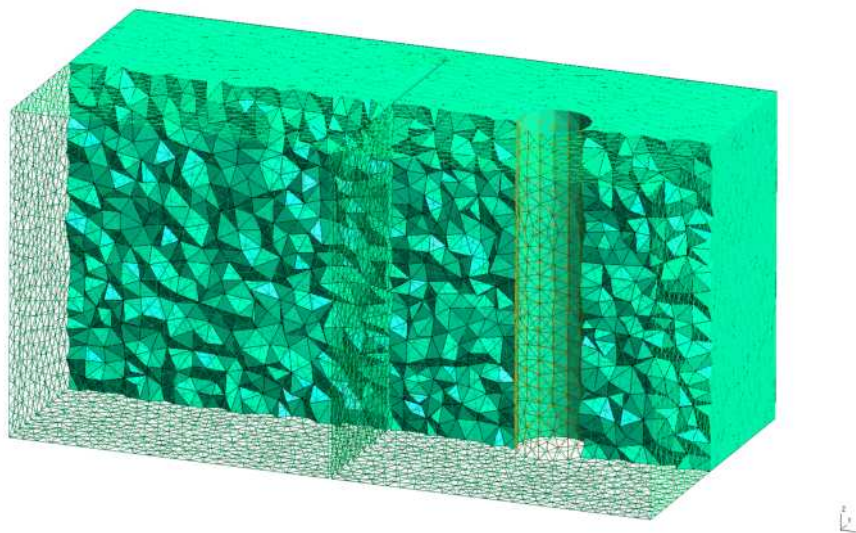
Figure 4: Tetrahedral mesh of the coupled cavities test-case containing the lossy cylinder.

5 Results

EDM results are presented in Sections 5.1 to 5.4 for baseline canonical test cases with the following parameters:

- The Sabine EC (1.17) is used for all surfaces;

- For the loaded cases the diffusivity is determined using (1.10);

- The specularity factor (1.14) is taken to be unity.

For coupled cavities results are reported for SDM and EEBC DDM methods. In each case it was verified that the FCBC and EEBC DDM gave the same results and likewise for the SDM and non-overlapping Schwarz DDM. Generally the FCBC and EEBC agreed to within the convergence tolerance requested (0.1 %) in the total energy density while the agreement between the SDM and Schwarz DDM was very slightly worse than the requested tolerance, which is due to the differences in the meshes. Derived parameters common to all the canonical test-case models are given in Table 2.

Parameter	Unit	Value
wallEC	m/s	2.0236×10^5
cylEC	m/s	7.1201×10^7
partEC	m/s	2.0236×10^5
holeEC	m/s	7.4948×10^7
holeArea	m^2	0.018000
holeTCS	m^2	0.0045000
cylArea	m^2	0.14137
cylACS	m^2	0.033576

Table 2: Common derived parameters for the test-cases.

5.1 Empty unpartitioned cavity

The derived parameters for the empty unpartitioned cavity are given in Table 3 and the summary statistics for the average power density in the EDM models are presented in Table 4. Results are given for 2D and 3D SDM cases and also for the homogeneous PWB model. The power density is very uniform, with a coefficient of variation (COV) of about 0.6 %. All the models are in close agreement as expected, since the loss in the cavity is very low.

Parameter	Unit	Value
wallArea	m^2	2.025
cavityArea	m^2	2.025
cavityVolume	m^3	0.18225
wallMFP	m	0.36
cavityMFP	m	0.36
wallD	m^2/s	3.5975×10^7
cavityD	m^2/s	3.5975×10^7
wallACS	m^2	0.0013669
cavityACS	m^2	0.0013669

Table 3: Derived parameters for the unpartitioned empty cavity.

The variation of the power density in the z-direction is shown in Figure 5(a) at $y = L_y/2$ and various values of x. In this case the quadratic anzatz used in the Kantorovich reduction is seen to be quite accurate and the 2D model provides very good results. The variation of the power density in the x-direction for $z = L_z/2$ and a number of y positions is shown in Figure 5(b). The power density falls monotonically along the cavity away from the source as expected for a harmonic solution of the Laplace operator. At the source end of the cavity the EDM predicts higher power density than PWB, while at the opposite end the EDM result is lower than the PWB result. The average power density in the EDM in Table 4 is very close to the PWB prediction. The probability density function (PDF) for the average power density in the cavity is shown in Figure 5(c); it is a narrow monomodal distribution.

Figure 6 shows maps of various quantities in the $z = L_z/2$ plane. The power density is shown in Figure 6(a) as a hybrid heat and contour map; the power density is seen to be relative uniform in the y-direction away from the source. The uniformity shown in Figure 6(b) is the ratio of the EDM and PWB power densities. The zero isoline is located at approximately $x = 0.35$, indicating that in 65 % of the cavity the EDM power density is lower than the PWB power density. The anisotropy of the power
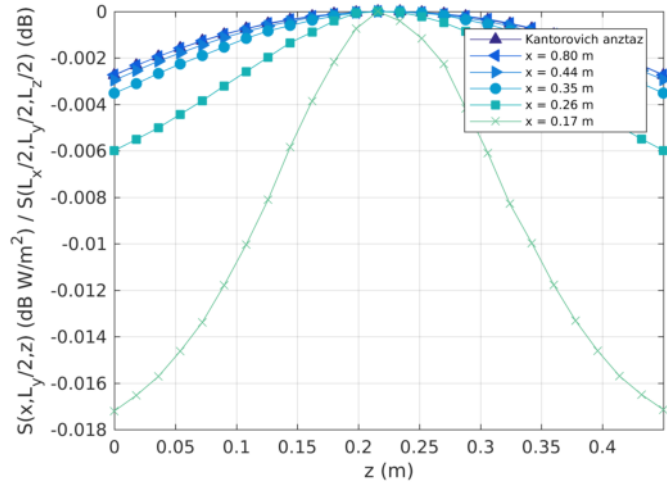
(a)
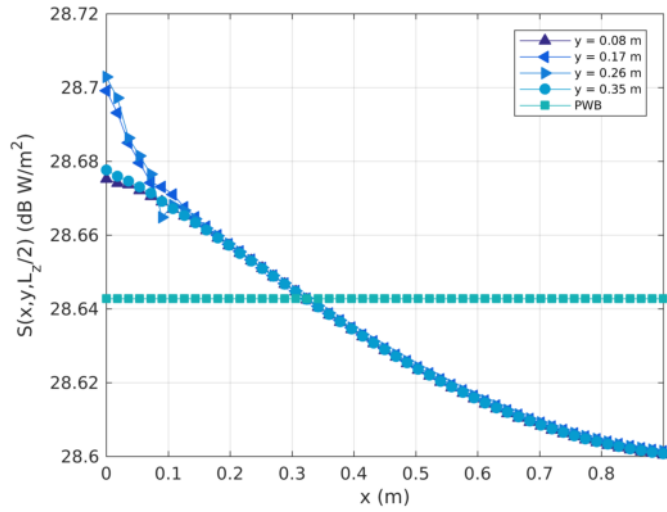
(b)
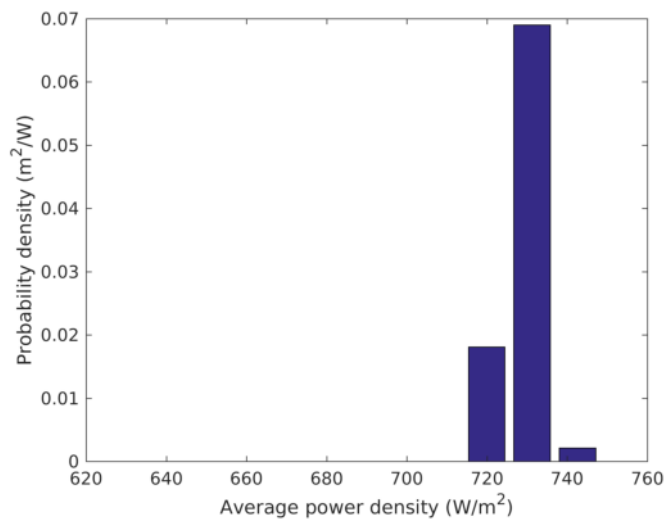
(c)

Figure 5: EDM of the unloaded unpartitioned cavity: (a) Normalised vertical profile of the power density; (b) Power density profile in the x-direction along the cavity centre; (c) PDF of the power density throughout the cavity volume.
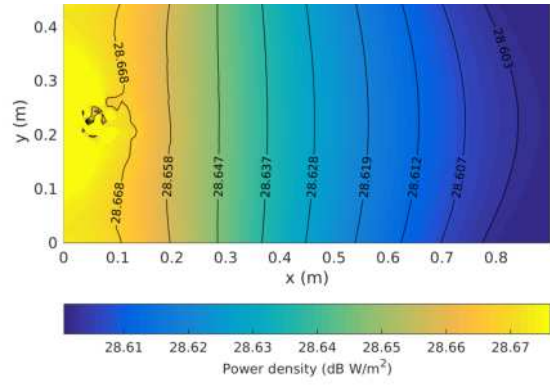
(a)
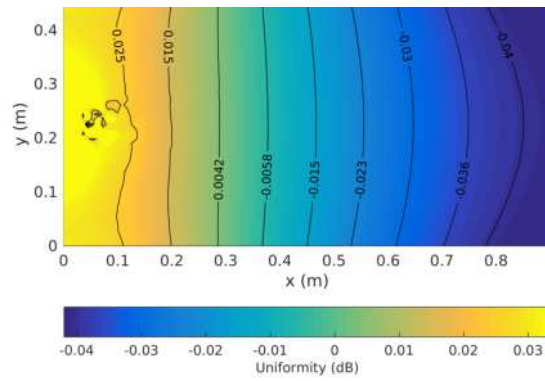
(b)
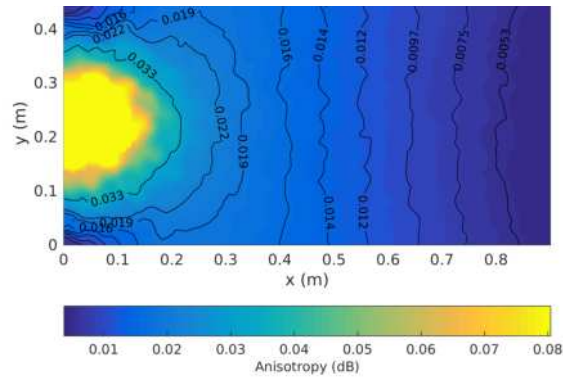
(c)
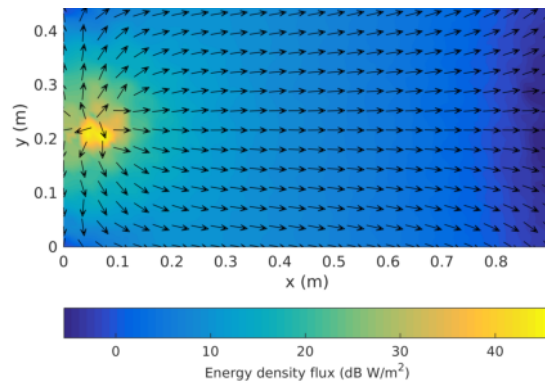
(d)

Figure 6: 3D EDM maps in the z-normal plane at the half height of the cavity for the unloaded unpartitioned cavity: (a) Power density; (b) Energy density relative to the homogeneous PWB model; (c) Anisotropy; (d) Energy density flux.

Power density	PWB	EDM	
		2D SDM	3D SDM
Value at centre (dB W m^{-2})	28.64	28.63	28.63
Mean (dB W m^{-2})	28.64	28.63	28.63
Minimum (dB W m^{-2})	28.64	28.60	28.03
Maximum (dB W m^{-2})	28.64	28.71	28.74
Standard deviation (dB W m^{-2})	0	6.50	6.17
Coefficient of variation (%)	0	0.61	0.57

Table 4: Statistics of the reverberant power density in the unpartitioned empty cavity.

density is defined as

$$\Upsilon(\mathbf{r}) = \frac{c_0 w(\mathbf{r})}{c_0 w(\mathbf{r}) - |\mathbf{J}(\mathbf{r})|} \tag{5.1}$$

and is shown in Figure 6(c); necessarily it must be greater close to the source. In most of the cavity the anisotropy is less than 0.05 dB. Figure 6(c) shows the flux of the energy density as a hybrid heat and vector field map with the colour indicating the magnitude and the arrow the direction. The flux is again relatively uniform away from the source and directed in the positive x-direction.

5.2 Unpartitioned cavity with a cylinder

The derived parameters for the loaded unpartitioned cavity are given in Table 5 and the corresponding summary statistics for the average power density in the EDM models are presented in Table 6. Results are given for 2D and 3D SDM cases and also for the homogeneous PWB model. The power density varies significantly in the volume of the cavity with a coefficient of variation (COV) of about 23,%. The 2D and 3D EDM are still in close agreement but diverge from the homogeneous PWB prediction. Even the average EDM power density of 14.3 dB W m^{-2} deviates significantly from the PWB value of 11.9 dB W m^{-2}. This result was verified using an independently constructed EDM of the specific test-case.

Parameter	Unit	Value
wallArea	m^2	2.0093
cavityArea	m^2	2.1507
cavityVolume	m^3	0.17872
wallMFP	m	0.35578
cylMFP	m	5.0566
cavityMFP	m	0.33239
wallD	m^2/s	3.5553×10^7
cylD	m^2/s	5.0531×10^8
cavityD	m^2/s	3.3216×10^7
wallACS	m^2	0.0013563
cavityACS	m^2	0.034932

Table 5: Derived parameters for the unpartitioned loaded cavity.

The variation of the power density in the z-direction is shown in Figure 7(a) at $y = L_y/2$ and various values of x. In this case the quadratic anzatz used in the Kantorovich reduction is seen to be less
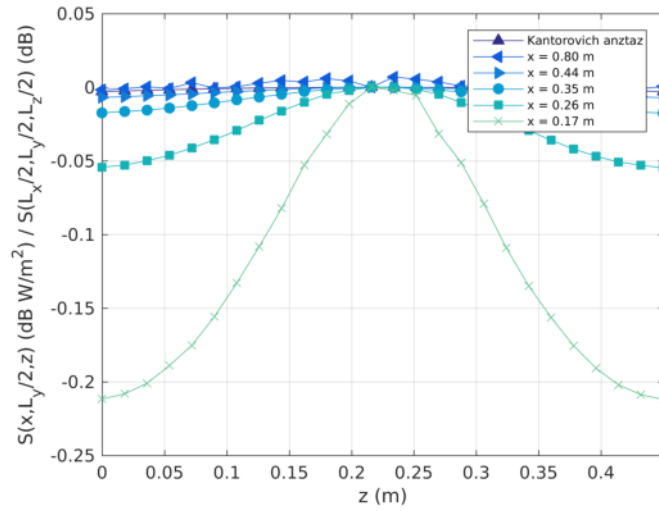
(a)
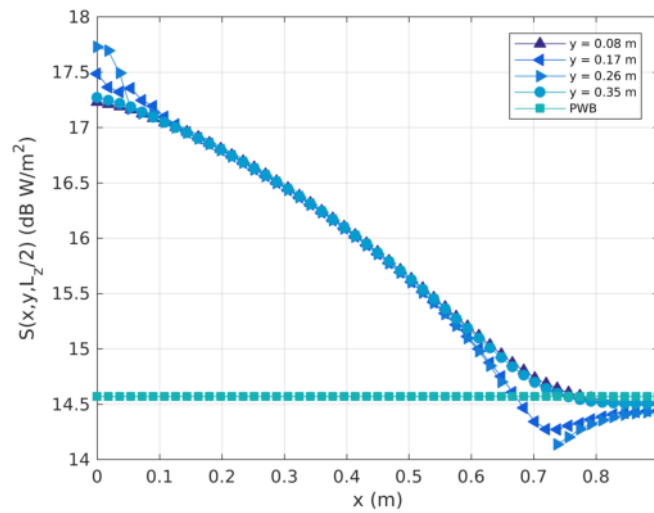
(b)
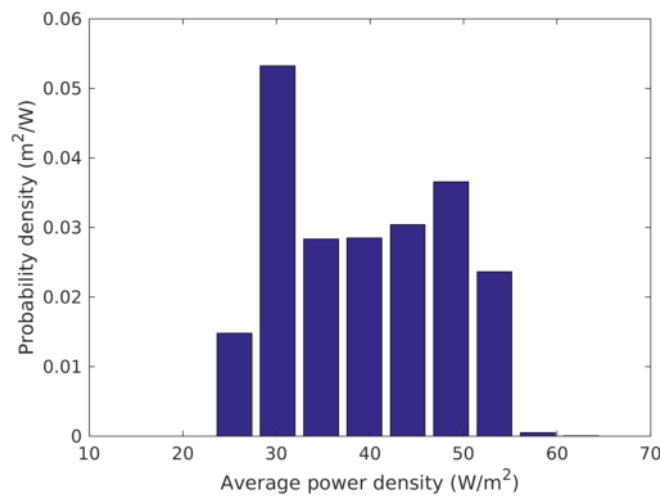
(c)

Figure 7: EDM of the loaded unpartitioned cavity: (a) Normalised vertical profile of the power density; (b) Power density profile in the x-direction along the cavity centre; (c) PDF of the power density throughout the cavity volume.

(a)

(b)

(c)

(d)

Figure 8:   3D EDM maps in the z-normal plane at the half height of the cavity for the loaded unpartitioned cavity: (a) Power density; (b) Energy density relative to the homogeneous PWB model; (c) Anisotropy; (d) Energy density flux.

Power density	PWB	EDM	
		2D SDM	**3D SDM**
Value at centre (dB W m^{-2})	14.57	15.90	15.85
Mean (dB W m^{-2})	14.57	16.00	15.93
Minimum (dB W m^{-2})	14.57	14.12	12.69
Maximum (dB W m^{-2})	14.57	17.72	18.12
Standard deviation (dB W m^{-2})	0	9.54	9.37
Coefficient of variation (%)	0	22.6	22.1

Table 6: Statistics of the reverberant power density in the unpartitioned cavity with the cylinder.

accurate; however, the 2D model still provides good results. The variation of the power density in the x direction for $z = L_z/2$ and a number of y positions is shown in Figure 5(b). The power density again falls monotonically along the cavity away from the source. At the source end of the cavity the EDM predicts higher power density than PWB, while at the opposite end the EDM result is a little lower than the PWB result. The average power density in the EDM in Table 4 is 1.5 dB higher than the PWB prediction. The probability density function (PDF) for the average power density in the cavity is shown in Figure 5(c); it is a relatively uniform distribution.

Figure 8 shows maps of various quantities in the $z = L_z/2$ plane. The power density shown in Figure 8(a) exhibits a monotonic decrease along the cavity, with a shadow region behind the cylinder. The uniformity shown in Figure 8(b) is the ratio of the EDM and PWB power densities. The zero isoline is close to the cylinder indicating that in most of the cavity the EDM power density is higher than the PWB power density. The anisotropy of the power density is shown in Figure 8(c); it is much higher than for the unloaded cavity with a typically value of 0.5 dB. Figure 8(c) shows the flux of the energy density, which clearly shows the flow of reverberant power from the source to the cylinder.

5.3 Empty partitioned cavity

The derived parameters empty for the partitioned cavity are given in Table 7 and the summary statistics for the average power density in the EDM models are presented in Table 8. Results are given for 2D and 3D SDM cases, EEBC and SDM models for the hole, and also for the homogeneous PWB model.

The power density is fairly uniform within each sub-cavity, with a COV of about 0.65 % in the source cavity and a slightly lower value of 0.45 % in the coupled cavity. The 2D and 3D models are in very close agreement and the EEBC and SDM models only differ by about 1 %.

The variation of the power density in the z-direction for the SDM and EEBC models are shown in Figure 9(a) and Figure 11(a) at $y = L_y/2$ and various values of x. In this case the quadratic anzatz used in the Kantorovich reduction is seen to be quite accurate and the 2D model provides very good results. The variation of the power density in the x direction for $z = L_z/2$ and a number of y positions is shown in Figure 9(b) and Figure 11(b) for the SDM and EEBC. The power density is relatively uniform in each sub-cavity, falling slightly towards the hole in the source sub-cavity and away from the hole in the coupled sub-cavity. In both cases there is a rapid variation in the average power at the hole; however, there is a significant difference in the level between the sub-cavities predicted by the SDM and EEBC methods of treating the aperture BC. The SDM predicts a much small level difference than the EEBC. The level difference predicted by the EEBC model is quite close to the PWB model prediction. Forcing continuity of both the energy density and its flux appears to constrain the level difference between the two cavities, while only enforcing continuity of the energy density flux allows a greater divergence. The probability density function (PDF) for the average power density in the sub-cavities are shown in Figure 9(c) and Figure 11(c).

Figure 10 and Figure 12 shows maps of various quantities in the $z = L_z/2$ plane for the SDM and EEBC models respectively. The power densities are shown in Figure 10(a) and Figure 12(a) as hybrid heat and contour maps; the power density is seen to fall off along the source sub-cavity towards the aperture and then in the coupled sub-cavity increase away from the hole. The uniformities in the SDM

Parameter	Unit	Source sub-cavity	Coupled sub-cavity
`wallArea`	m^2	1.0080	1.0080
`partArea`	m^2	0.1845	0.1845
`holeArea`	m^2	0.0180	0.0180
`cavityArea`	m^2	1.2105	1.2105
`cavityVolume`	m^3	0.090619	0.090619
`wallMFP`	m	0.35960	0.35960
`partMFP`	m	1.9646	1.9646
`cavityMFP`	m	0.29944	0.29944
`wallD`	m^2/s	3.5935×10^7	3.5935×10^7
`partD`	m^2/s	1.9633×10^8	1.9633×10^8
`cavityD`	m^2/s	2.9924×10^7	2.9924×10^7
`wallACS`	m^2	0.00068040	0.00068040
`partACS`	m^2	0.00012454	0.00012454
`cavityACS`	m^2	0.00080494	0.00080494

Table 7: Derived parameters for the unloaded partitioned cavity.

and EEBC models are shown in Figure 10(b) and Figure 12(b) as the ratio of the EDM and PWB power densities. In both cases the EDM predicts lower values than the PWB model in the source cavity and higher values in the coupled cavity. The anisotropies are shown in Figure 10(c) and Figure 12(c) and are fairly similar for the two aperture models, as are the energy density fluxes shown in Figure 10(c) and Figure 12(c).

5.4 Partitioned cavity with a cylinder

The derived parameters for the partitioned cavity loaded with the cylinder are given in Table 9 and the summary statistics for the average power density in the EDM models are presented in Table 10. Results are again given for 2D and 3D SDM cases, EEBC and SDM models for the hole, and also for the homogeneous PWB model.

The power density now varies significantly within each sub-cavity and the difference in level between the sub-cavities is also much greater. Again the 2D and 3D models are in reasonable agreement regarding the basic statistics of the average power density. The level difference between the SDM and EEBC models for the hole is now accentuated. The COV in the energy density in the source sub-cavity is about 6 % for the SDM model and only 2 % for the EEBC model. Note that this difference in COV is mainly due to the difference in the average energy densities between the two models. The COV in the coupled cavity is much higher at about 20 % for both the SDM and EEBC models, which are closer in absolute level in this sub-cavity.
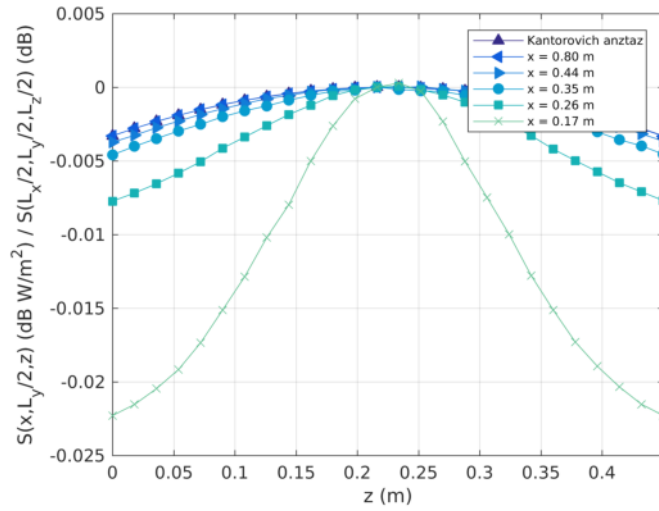
(a)
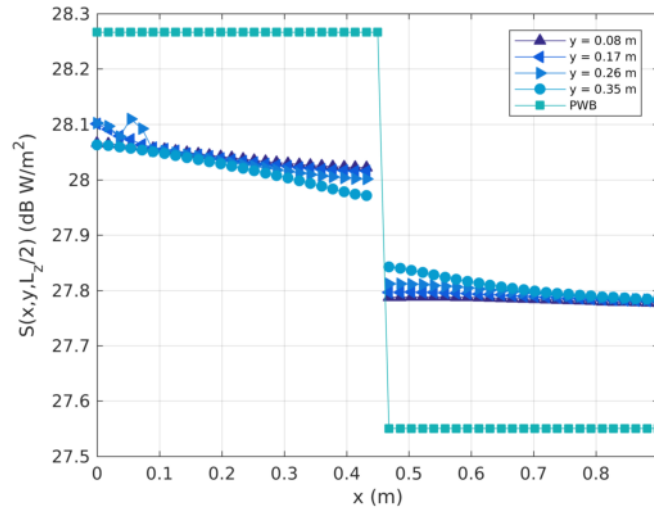
(b)
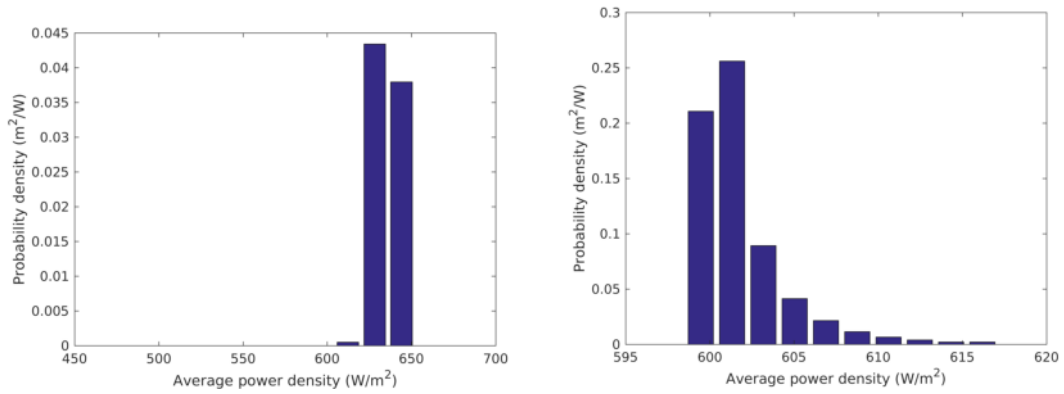
(c)

Figure 9: Single domain EDM of the unloaded partitioned cavity: (a) Normalised vertical profile of the power density; (b) Power density profile in the x-direction along the cavity centre; (c) PDF of the power density in the source cavity (left) and coupled cavity (right).
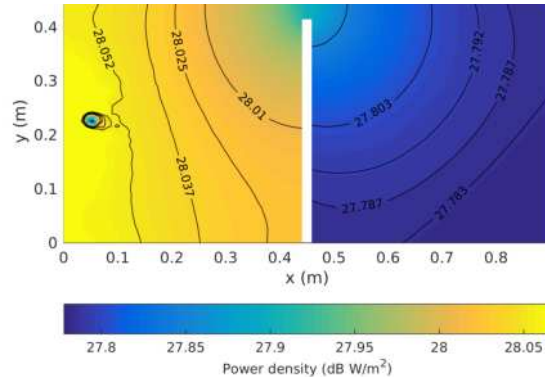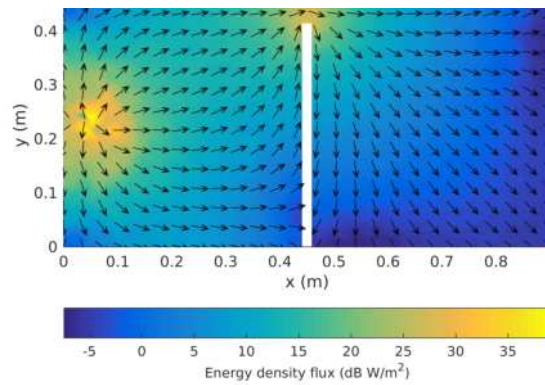
(a)
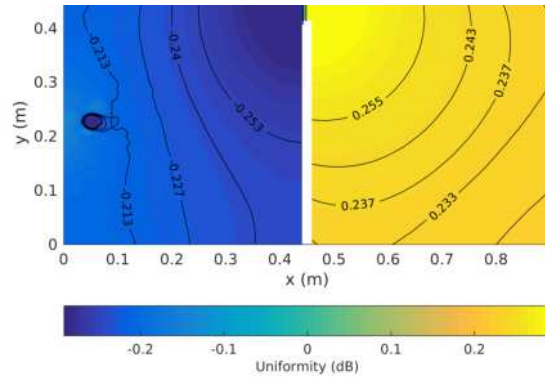
(b)
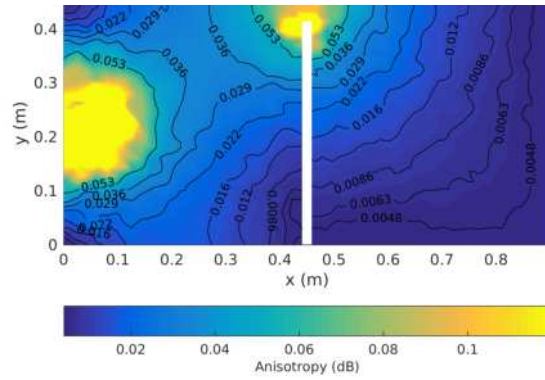
(c)
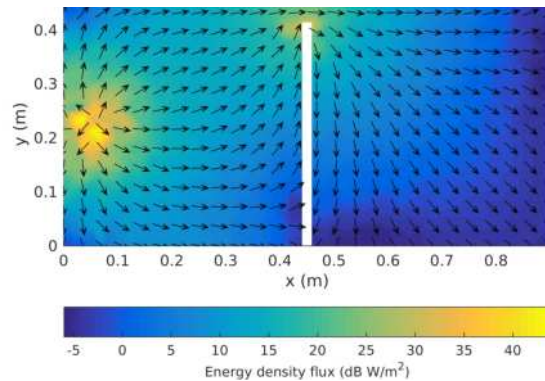
(d)

Figure 10: Single domain 3D EDM maps in the z-normal plane at the half height of the cavity for the unloaded partitioned cavity: (a) Power density; (b) Energy density relative to the homogeneous PWB model; (c) Anisotropy; (d) Energy density flux.
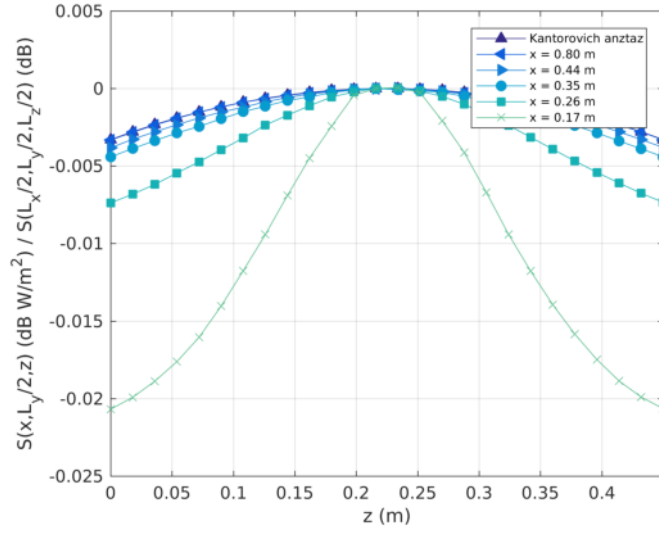
(a)
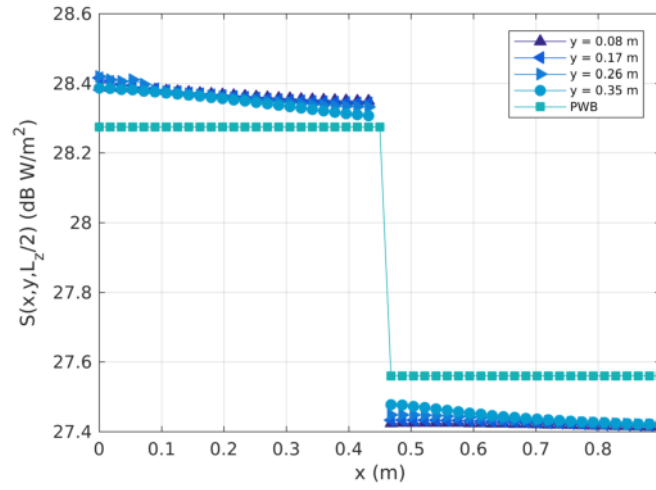
(b)
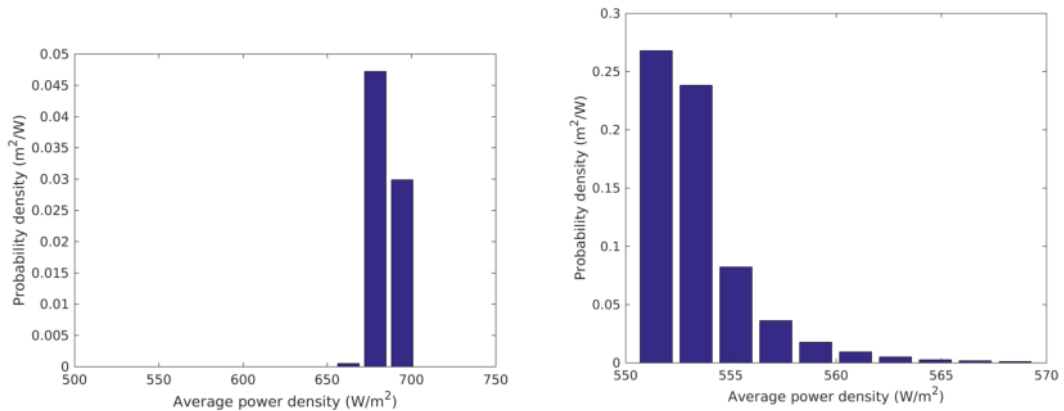
(c)

Figure 11: Dual domain EEBC EDM of the unloaded partitioned cavity: (a) Normalised vertical profile of the power density; (b) Power density profile in the x-direction along the cavity centre; (c) PDF of the power density in the source cavity (left) and coupled cavity (right).
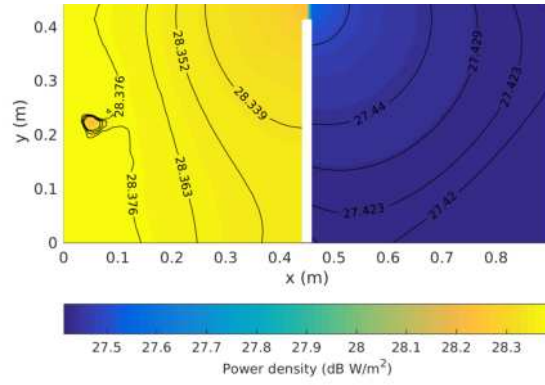
(a)
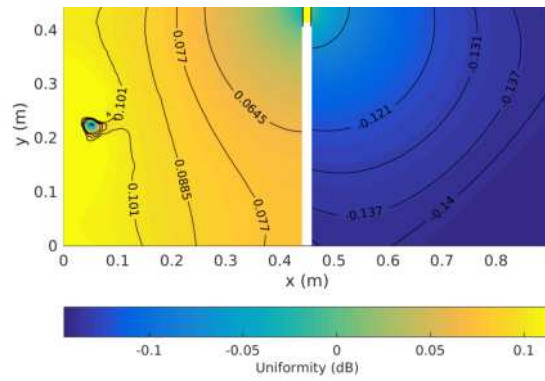
(b)
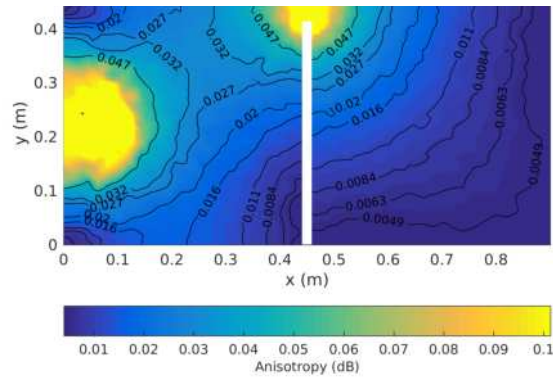
(c)

(d)

Figure 12: Dual domain EEBC 3D EDM maps in the z-normal plane at the half height of the cavity for the unloaded partitioned cavity: (a) Power density; (b) Energy density relative to the homogeneous PWB model; (c) Anisotropy; (d) Energy density flux.

Power density	PWB	EDM			
		2D SDM	**2D DDM**	**3D SDM**	**3D DDM**
Sub-cavity 1					
Value at centre (dB W m^{-2})	28.27	28.04	28.37	28.03	28.36
Mean (dB W m^{-2})	28.27	28.04	28.36	28.03	28.36
Minimum (dB W m^{-2})	28.27	27.89	28.24	26.93	27.35
Maximum (dB W m^{-2})	28.27	28.11	28.43	28.14	28.47
Standard deviation (dB W m^{-2})	0	6.47	6.28	5.95	5.76
Coefficient of variation (%)	0	0.70	0.62	0.62	0.55
Sub-cavity 2					
Value at centre (dB W m^{-2})	27.55	27.78	27.42	27.78	27.42
Mean (dB W m^{-2})	27.55	27.79	27.43	27.79	27.43
Minimum (dB W m^{-2})	27.55	27.76	27.41	27.77	27.41
Maximum (dB W m^{-2})	27.55	27.89	27.55	27.90	27.55
Standard deviation (dB W m^{-2})	0	4.17	3.85	4.16	3.85
Coefficient of variation (%)	0	0.44	0.44	0.43	0.44

Table 8: Statistics of the reverberant power density in the unloaded partitioned cavity.

Parameter	Unit	Source sub-cavity	Coupled sub-cavity
wallArea	m^2	1.0080	0.99229
partArea	m^2	0.18450	0.18450
holeArea	m^2	0.018000	0.018000
cavityArea	m^2	1.2105	1.3362
cavityVolume	m^3	0.090619	0.087084
wallMFP	m	0.35960	0.35104
partMFP	m	1.9646	1.8880
cavityMFP	m	0.29944	0.26070
wallD	m^2/s	3.5935×10^7	3.5080×10^7
partD	m^2/s	1.9633×10^8	1.8867×10^8
cylD	m^2/s	-	2.4623×10^8
cavityD	m^2/s	2.9924×10^7	2.6052×10^7
wallACS	m^2	0.00068040	0.00066980
partACS	m^2	0.00012454	0.00012454
cavityACS	m^2	0.00080494	0.034370

Table 9: Derived parameters for the loaded partitioned cavity.

Power density	PWB	EDM			
		2D SDM	2D DDM	3D SDM	3D DDM
Sub-cavity 1					
Value at centre (dB W m^{-2})	23.20	20.24	24.25	20.06	24.22
Mean (dB W m^{-2})	23.20	20.22	24.24	20.04	24.21
Minimum (dB W m^{-2})	23.20	18.36	23.66	18.18	20.89
Maximum (dB W m^{-2})	23.20	20.70	24.43	20.90	24.51
Standard deviation (dB W m^{-2})	0	8.24	7.78	7.91	7.46
Coefficient of variation (%)	0	6.36	2.26	6.13	2.11
Sub-cavity 2					
Value at centre (dB W m^{-2})	13.84	14.27	13.60	14.29	13.63
Mean (dB W m^{-2})	13.84	14.93	14.33	14.95	14.28
Minimum (dB W m^{-2})	13.84	13.80	13.09	13.84	13.16
Maximum (dB W m^{-2})	13.84	18.29	18.09	18.24	17.82
Standard deviation (dB W m^{-2})	0	7.94	7.73	7.92	7.30
Coefficient of variation (%)	0	20.0	21.9	19.8	20.0

Table 10: Statistics of the reverberant power density in the partitioned cavity with the cylinder.

The variation of the power density in the z-direction for the SDM and EEBC model are shown in Figure 13(a) and Figure 15(a) at $y = L_y/2$ and various values of x. In this case the quadratic anzatz used in the Kantorovich reduction is seen to be quite accurate away from the source and the 2D model provides very good results. Note, however that the vertical profile near the aperture ($x = 0.44$ m) for the EEBC is somewhat erratic, perhaps indicating some numerical issue. It must always be remembered that the EDM is not expected to valid very close to an aperture, where the field cannot be highly diffuse. The variation of the power density in the x-direction for $z = L_z/2$ and a number of y positions is shown in Figure 13(b) and Figure 15(b) for the SDM and EEBC. We again see that the SDM predicts less level difference between the two cavities than the EEBC and PWB models, which give comparable levels. The SDM result for the loaded cases is notably less symmetrically placed between the PWB levels than was the case for the unloaded cases. The EEBC model predicts a slightly higher power density in the source cavity and its average level is in reasonable agreement with the PWB model in the coupled cavity. The range of the power density in the coupled sub-cavity is about 2 dB for both the SDM and EEBC models with a similar profile. The PDF for the average power density in the sub-cavities are shown in Figure 13(c) and Figure 15(c).

Figure 14 and Figure 16 shows maps of various quantities in the $z = L_z/2$ plane for the SDM and EEBC model respectively. The power densities are shown in Figure 14(a) and Figure 16(a) as hybrid heat and contour maps; the power density again falls off along the source sub-cavity towards the aperture and then in the coupled sub-cavity increase away from the hole. The uniformities in the SDM and EEBC models are shown in Figure 14(b) and Figure 16(b). In both cases the EDM again predicts lower values than the PWB model in the source cavity and high values in the coupled cavity, as was the case for the unloaded partition cavity. The anisotropies are shown in Figure 14(c) and Figure 16(c) and are fairly similar for the two aperture models. The anisotropy varies up to about 1.5 dB in the cavity and notably remains above 1 dB in the volume of the coupled sub-cavity between the hole and the cylinder. The energy density fluxes shown in Figure 14(c) and Figure 16(c) are fairly similar in structure with some difference in magnitude due to the energy density division between the sub-cavities.
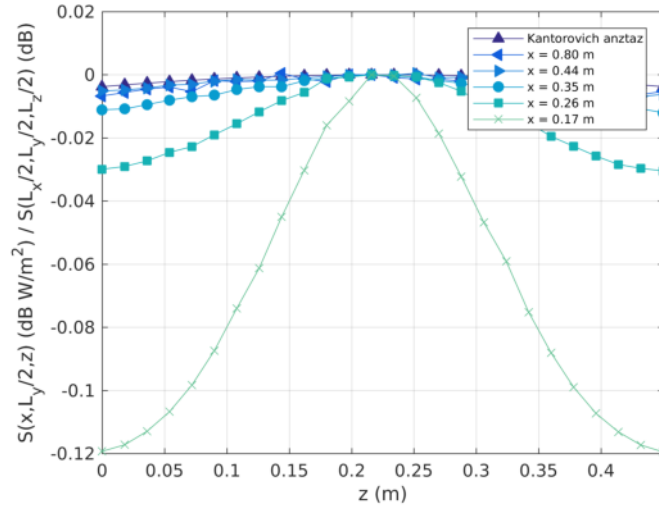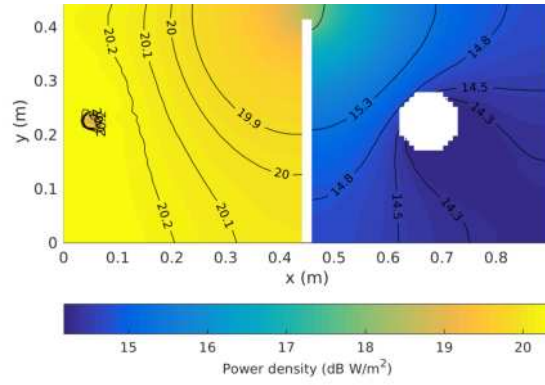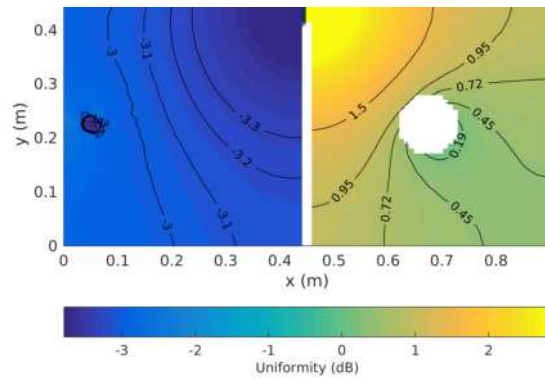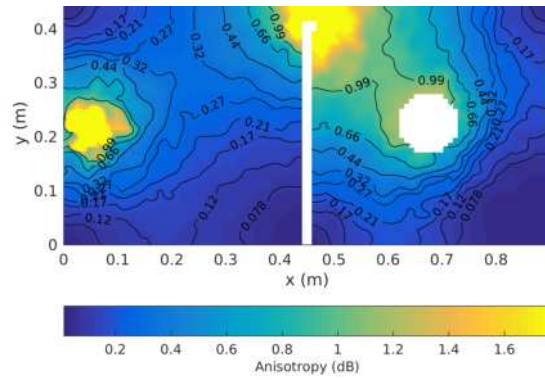
(a)
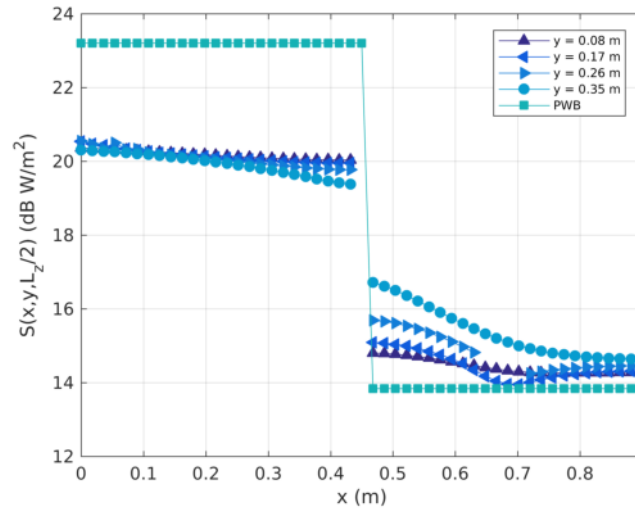
(b)
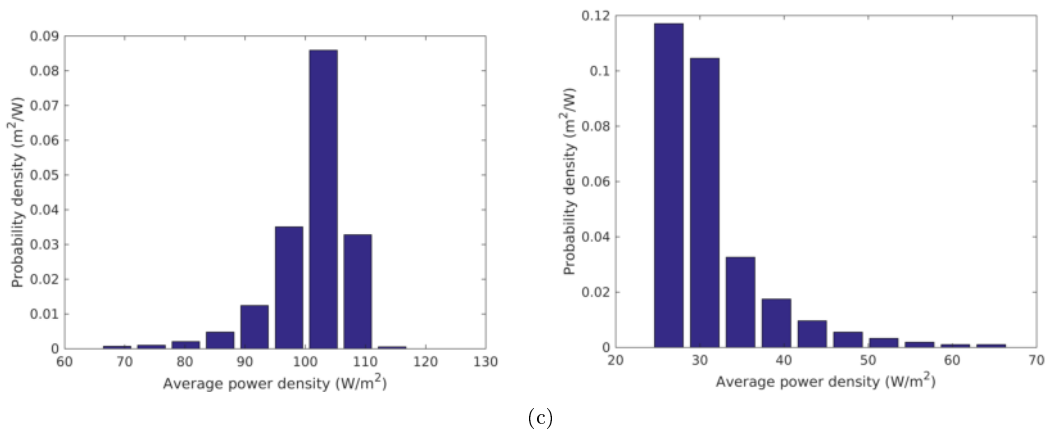
(c)

Figure 13: Single domain EDM of the loaded partitioned cavity: (a) Normalised vertical profile of the power density; (b) Power density profile in the x-direction along the cavity centre; (c) PDF of the power density in the source cavity (left) and coupled cavity (right).
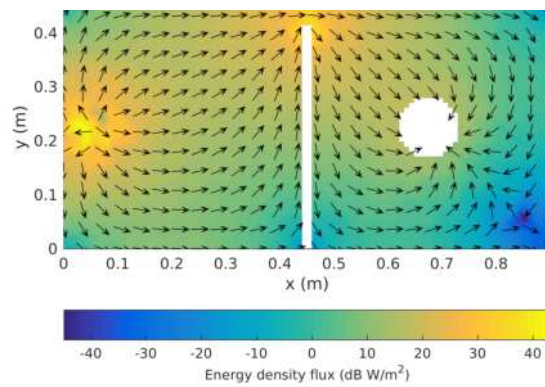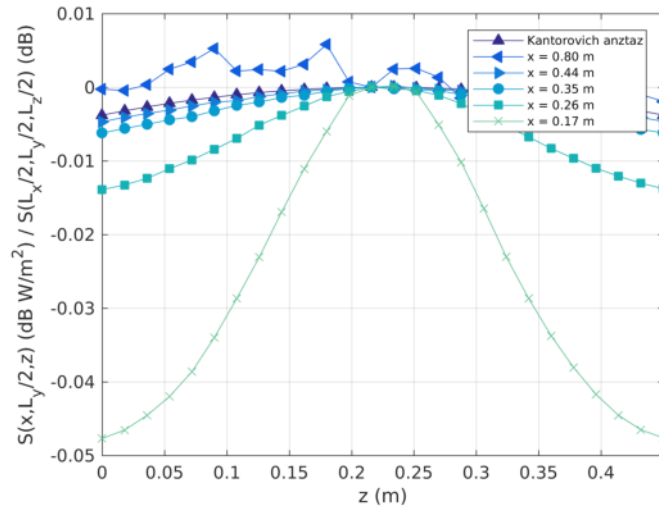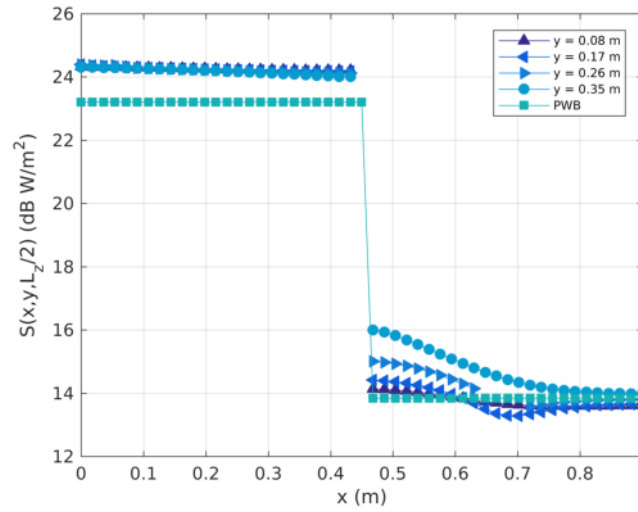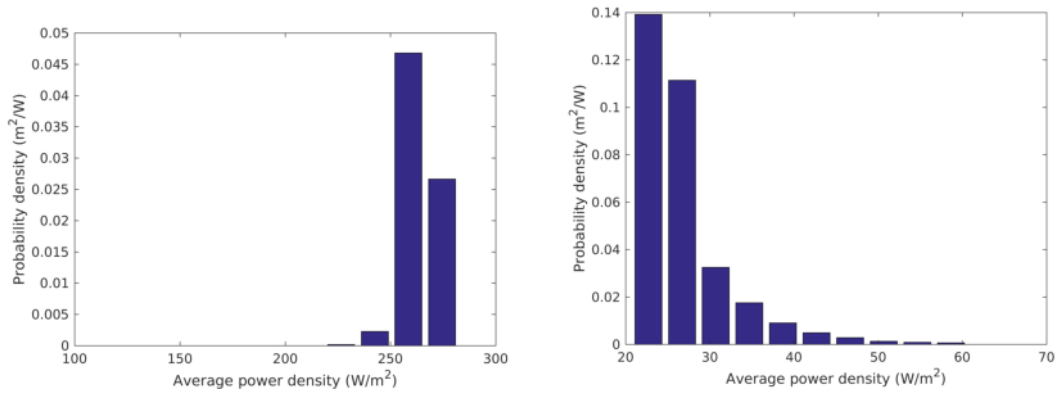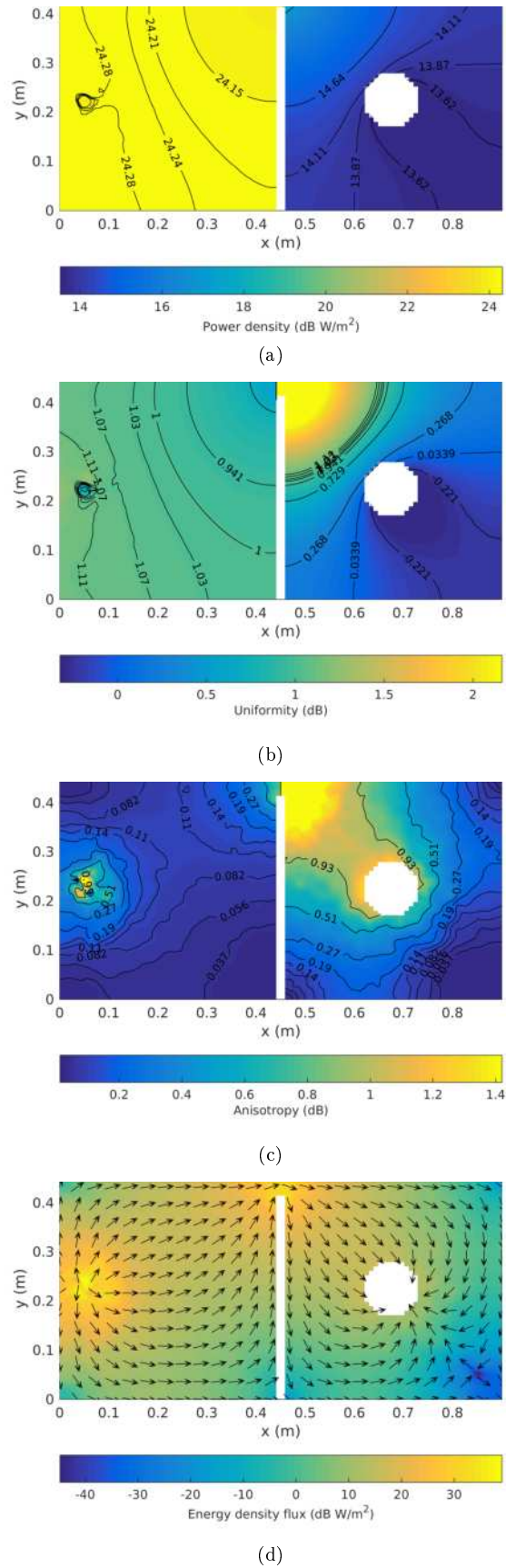
(a)

(b)

(c)

(d)

Figure 14:   Single domain 3D EDM maps in the *z*-normal plane at the half height of the cavity for the loaded partitioned cavity: (a) Power density; (b) Energy density relative to the homogeneous PWB model; (c) Anisotropy; (d) Energy density flux.

(a)

(b)

(c)

Figure 15: Dual domain EEBC EDM of the loaded partitioned cavity: (a) Normalised vertical profile of the power density; (b) Power density profile in the x-direction along the cavity centre; (c) PDF of the power density in the source cavity (left) and coupled cavity (right).

(a)

(b)

(c)

(d)

Figure 16: Dual domain EEBC 3D EDM maps in the z-normal plane at the half height of the cavity for the loaded partitioned cavity: (a) Power density; (b) Energy density relative to the homogeneous PWB model; (c) Anisotropy; (d) Energy density flux.

5.5 Comparison to measurements

Measurements of the power density in a physical implementation of the test-cases where reported in (Flintoft et al., 2017). In this section this measurement data is compared to the predictions of the 3D EDM. Since it is readily apparent that the SDM model of the partitioned cavity does not agree well with the measurement data only the 3D EEBC model results are considered. EDM results with two different EC models, Sabine and Jing and Xiang, are however shown. The comparisons are made using the profile of the power density in the x direction along the cavity.

Figure 17 shows the power density comparison for the unloaded unpartitioned cavity. The measurement result exhibits significant statistical variation. The EDM results are at least consistent with the measurement data in this case and no conclusion can be draw regarding the validity of the two EC models.
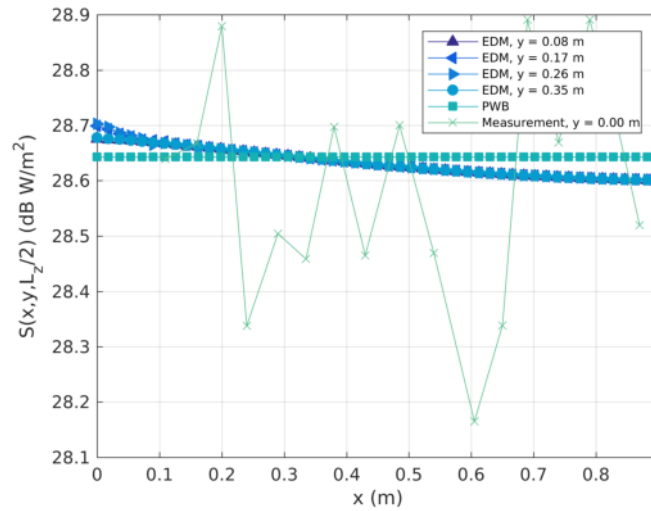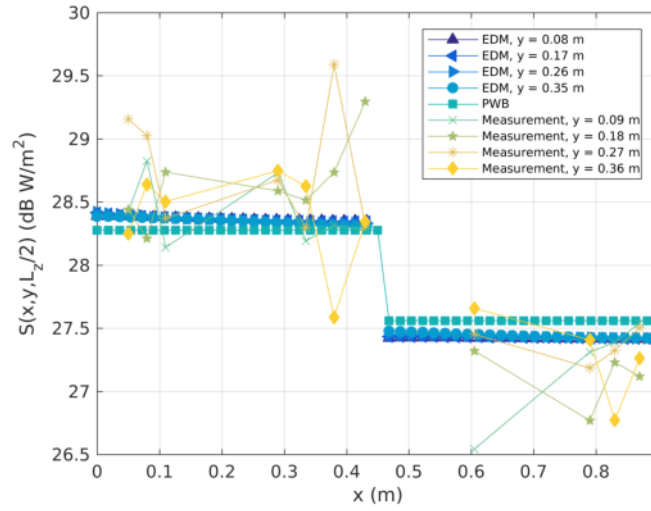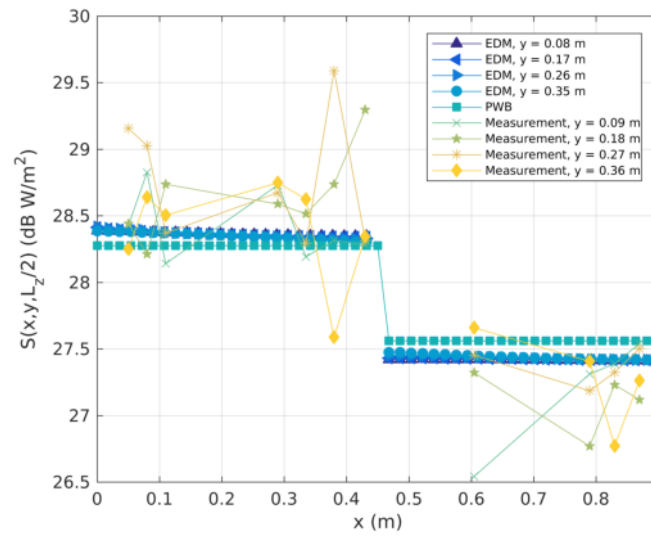

(a)
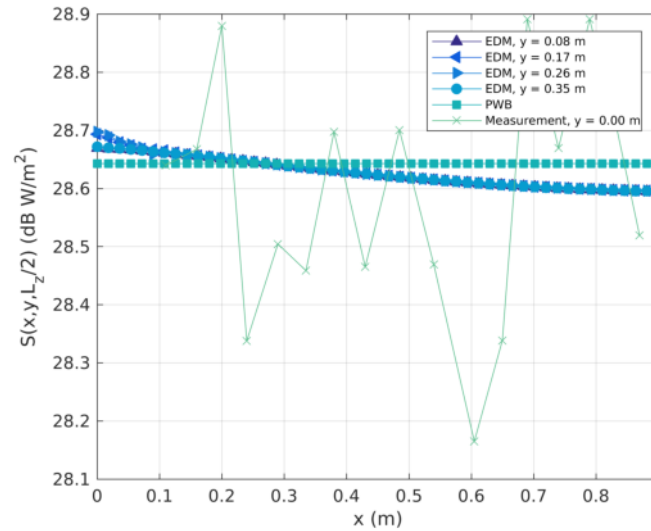
(b)

Figure 17: Power density profile in the x-direction along the cavity centre comparing the 3D EDM of the single unloaded cavity and measurement (Flintoft et al., 2017): (a) Sabine EC; (b) Jing and Xiang EC.

Figure 18 shows the power density comparison for the loaded unpartitioned cavity. While again the measurement has significant statistical variation, the general trend of the measurement data, a reduction in level with increasing distance from the source, is consistent with the EDM results. While neither EC model matches the overall trend in the measurement across the full length of the cavity, the measurement data is generally within the range of the two models, favouring te Sabine EC model closer to the source and the Jing and Xiang model at the other end of the cavity.
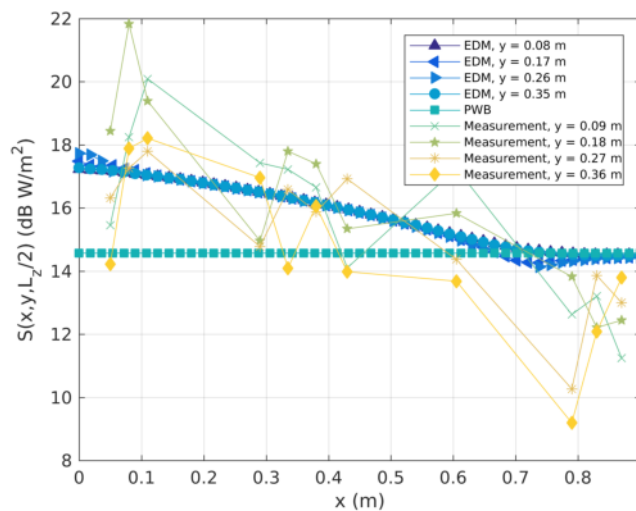
(a)
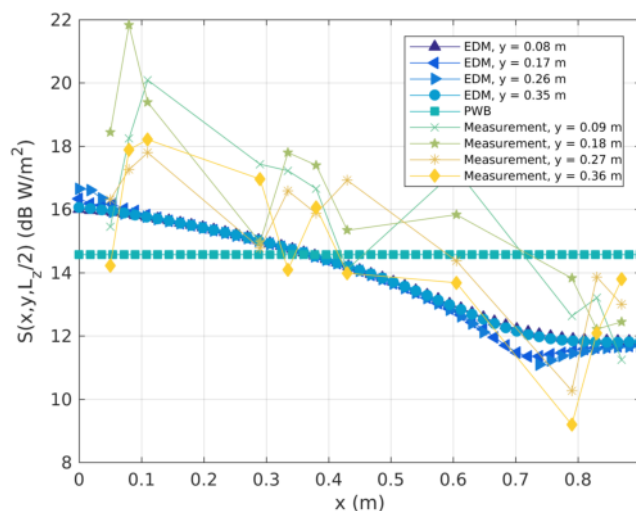
(b)

Figure 18: Power density profile in the x-direction along the cavity centre comparing the 3D EDM of the single loaded cavity and measurement (Flintoft et al., 2017): (a) Sabine EC; (b) Jing and Xiang EC.

The power density comparison for the unloaded partitioned cavity is shown in Figure 19. Since the loss is low the Sabine and Jing and Xiang EC models give very similar results. The agreement with the measurement data is good, though the EDM seems to overestimate the power density in the coupled cavity. The statistical variation of the measurement data is a least consistent with a relatively uniform level in each sub-cavity.

Figure 20 shows the power density comparison for the loaded partitioned cavity. In this case it appears that the simulation using the Jing and Xiang EC gives significantly better agreement with the
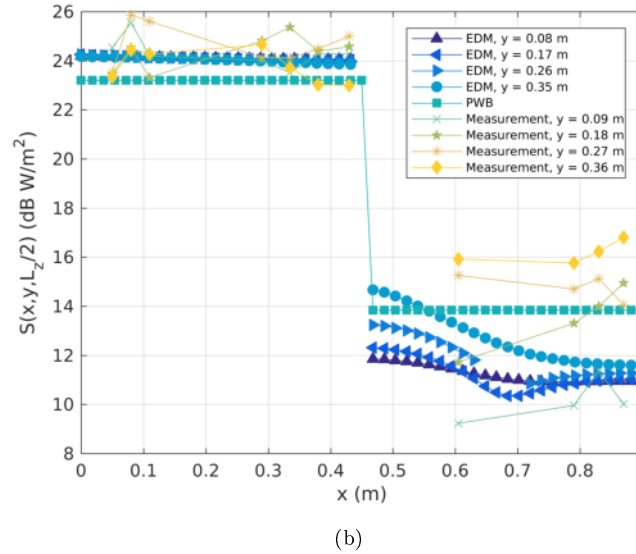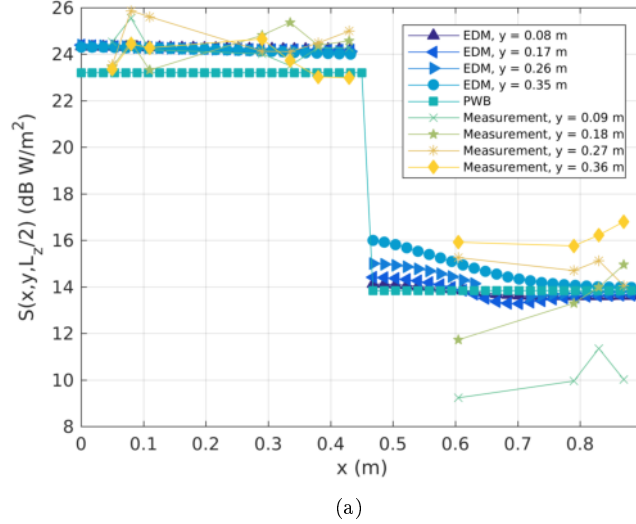
(a)

(b)

Figure 19: Power density profile in the x-direction along the cavity centre comparing the 3D DDM EEBC EDM of the dual unloaded cavity and measurement (Flintoft et al., 2017): (a) Sabine EC; (b) Jing and Xiang EC.

measurement data than the simulation using the Sabine EC model. The Sabine model appears to under-estimate the level difference between the cavities and shows less variation in the y direction than the measurement data. The Jing and Xiang EC simulation gives a much better estimate of the level difference and while it still under-estimates the variation in the y-direction compared to the measurement data, it is closer to the measurement than the prediction of the Sabine EC simulation.

(a)

(b)

Figure 20: Power density profile in the x-direction along the cavity centre comparing the 3D DDM EEBC EDM of the dual loaded cavity and measurement (Flintoft et al., 2017): (a) Sabine EC; (b) Jing and Xiang EC.

5.6 Parametric study

All the EDM simulations so far have assumed that the domain boundaries have completely diffuse reflections, corresponding to $\kappa = 1$ in (1.14). In this section a comparison is made between the measurement data from (Flintoft et al., 2017) and the 3D EDM (using the EEBC for the partitioned cavity and Jing and Xiang EC) with the specularity parameter κ taking values of 0.5, 0.75, 1, 1.5 and 2. Whilst in the acoustics diffusion model κ is supposed to quantify the effect of specular reflections on the diffusivity, in more general terms it represents variations in the MFP from the value given by that in (1.6).

Figure 21 shows the parametric sweep for the empty unpartitioned cavity. In this case there is little variation with κ and the statistical variation in the measurement data is too high to draw any conclusions. Figure 22 show the sweep for the loaded unpartitioned cavity. This shows that increasing κ tends to reduce both the overall level and variability in the power density in the cavity. The best comparison to the measurement data would appear to be achieved with κ in the range 0.5 to 0.75, with the lower value favoured.

The parametric sweep for the empty partitioned cavity is shown in Figure 23. As for the unloaded unpartitioned cavity the effect of κ is fairly small; however, lower values tend to increase the level difference and variability which is again more consistent with the measurement results. Figure 24 shows the sweep for the loaded partitioned cavity. The general behaviour is the same, with reducing κ increasing the level difference between the sub-cavities and increasing the variability within each sub-cavity. The best agreement with the measurement data is achieved with $\kappa \approx 0.5$.

6 Conclusions

The EDM can be implemented very efficiently in 2D and 3D using the FEM with FreeFEM++. For 2D models the geometry and mesh can be quickly generated within FreeFEM++ using its native CAD and mesh creation capabilities while for 3D models it was found to be more convenient and efficient to use Gmsh to create parametric CAD models and the 3D tetrahedral meshes needed by FreeFEM++. Typical solution times on a modern PC times for the test-case models are under a second for 2D and single domain models and a few seconds for 3D models.

The Kantorovich reduction of geometries with a predominately uniform cross-section along one direction was found to generally give good results compared to the full 3D model except in the immediate vicinity of the source. The quadratic vertical profile used as an anzatz in the 2D model was confirmed by the results of the 3D models.

For the test-cases without the cylinder the EDM gives very similar levels to the PWB model, with low variability in the power density. For the loaded test-cases variations of a few decibels in the average power density are predicted by the EDM, which are consistent with measurements. The hole between the two sub-cavities of the partitioned cavity was represented in two ways in the EDM - using a single cavity or using an EEBC. The measurement data is more consistent with the EEBC model for these test-cases in which the hole's width is about a wavelength at the central frequency of the measurement band. This suggest the hole is not electrically large enough for the two sub-cavities to be considered as a single diffuse volume and the hole is a pinch point, causing a discontinuity in the average energy density. A systematic analysis of the effect of the aperture size on the applicability of the different EDM models is required.

The measurement results generally compared well with the EDM simulations using the EEBC for the partitioned case and the Jing and Xiang EC. The main discrepancy was found in the variation of the power density in the coupled cavity when loaded with the cylinder. The measurements predicted greater variation in the transverse y-direction than predicted by the EDM. Adjusting the specularity factor κ to 0.5 tended to give a better comparison to the measurements in this case. In the ADM κ is adjusted to values greater than unity to account for increasing specularity in the surface reflections within a cavity. Here, it could be the the better agreement with $\kappa \sim 0.5$ is in fact indicative of a poor estimate of the cavity MFP by (1.6) when the cylinder is present. Perhaps the cylinder is so large that it changes the topology of the cavity significantly, resulting in a signiifcantly shorter MFP.

References

A. Billon, C. Foy, J. Picaut, V. Valeau, and A. Sakout. Modeling the sound transmission between rooms coupled through partition walls by using a diffusion model. *The Journal of the Acoustical Society of America*, 123(6):4261–4271, 2008. doi:10.1121/1.2905242.

M. Discacciati, A. Quarteroni, and A. Valli. Robin–robin domain decomposition methods for the stokes–darcy coupling. *SIAM Journal on Numerical Analysis*, 45(3):1246–1268, 2007. doi:10.1137/06065091X.
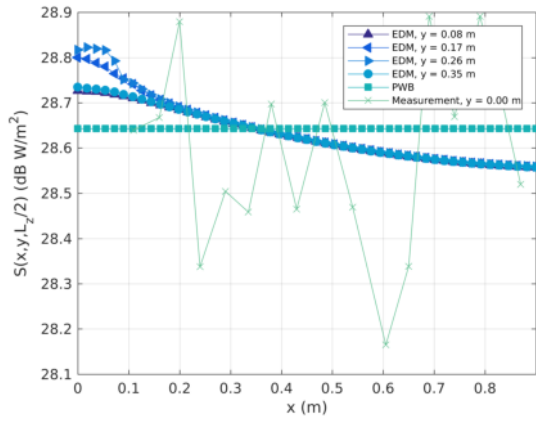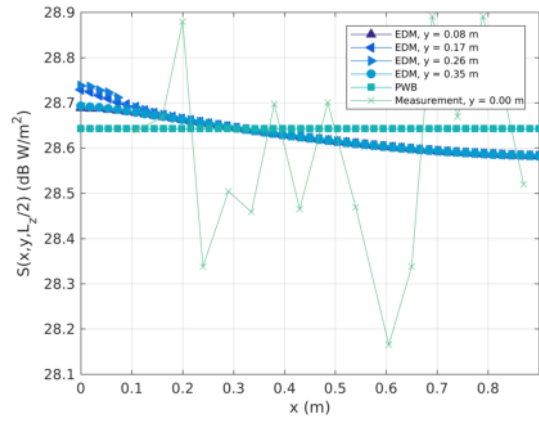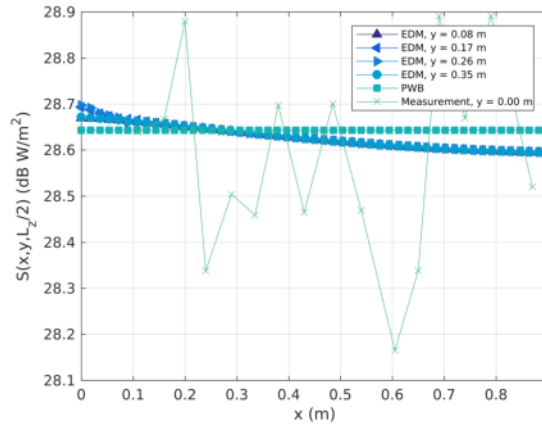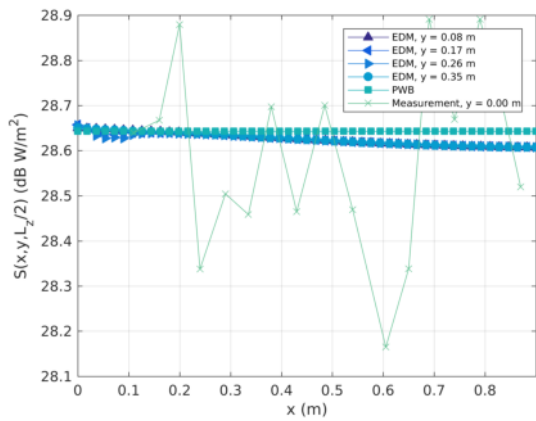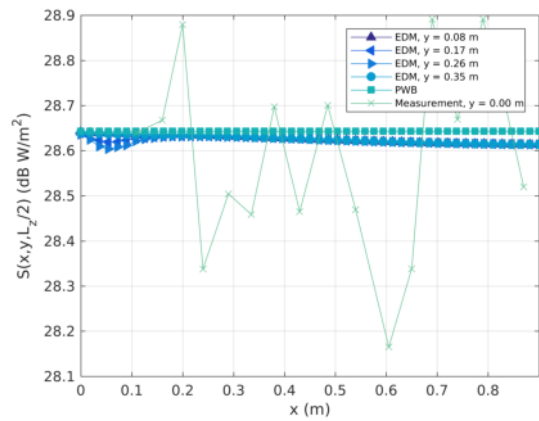
Figure 21: Power density profile in the x-direction along the cavity centre comparing the 3D EDM of the single unloaded cavity and measurement (Flintoft et al., 2017): (a) $\kappa = 1/2$; (b) $\kappa = 3/4$; (c) $\kappa = 1$; (d) $\kappa = 3/2$; (e) $\kappa = 2$.
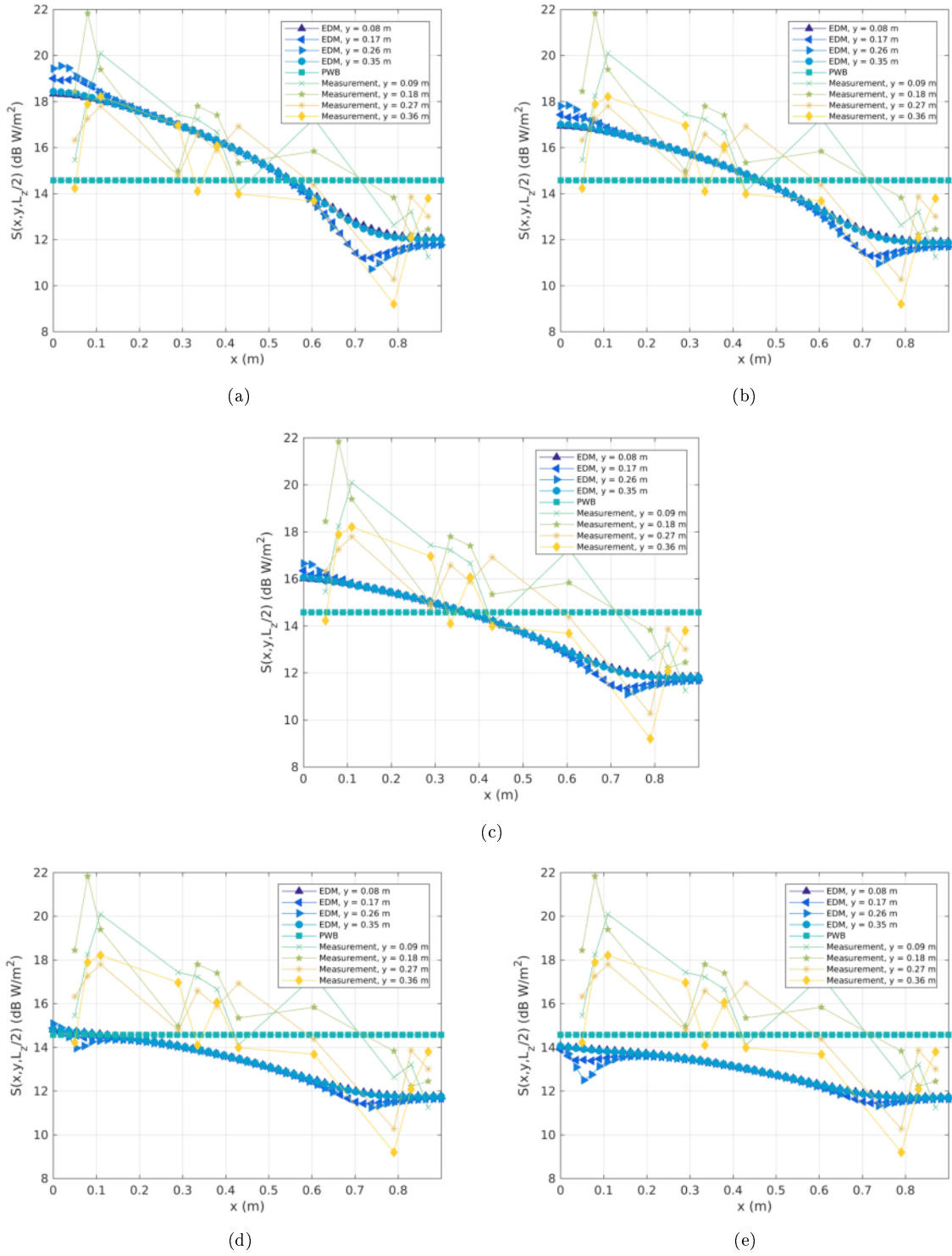
Figure 22: Power density profile in the x-direction along the cavity centre comparing the 3D EDM of the single loaded cavity and measurement (Flintoft et al., 2017): (a) $\kappa = 1/2$; (b) $\kappa = 3/4$; (c) $\kappa = 1$; (d) $\kappa = 3/2$; (e) $\kappa = 2$.
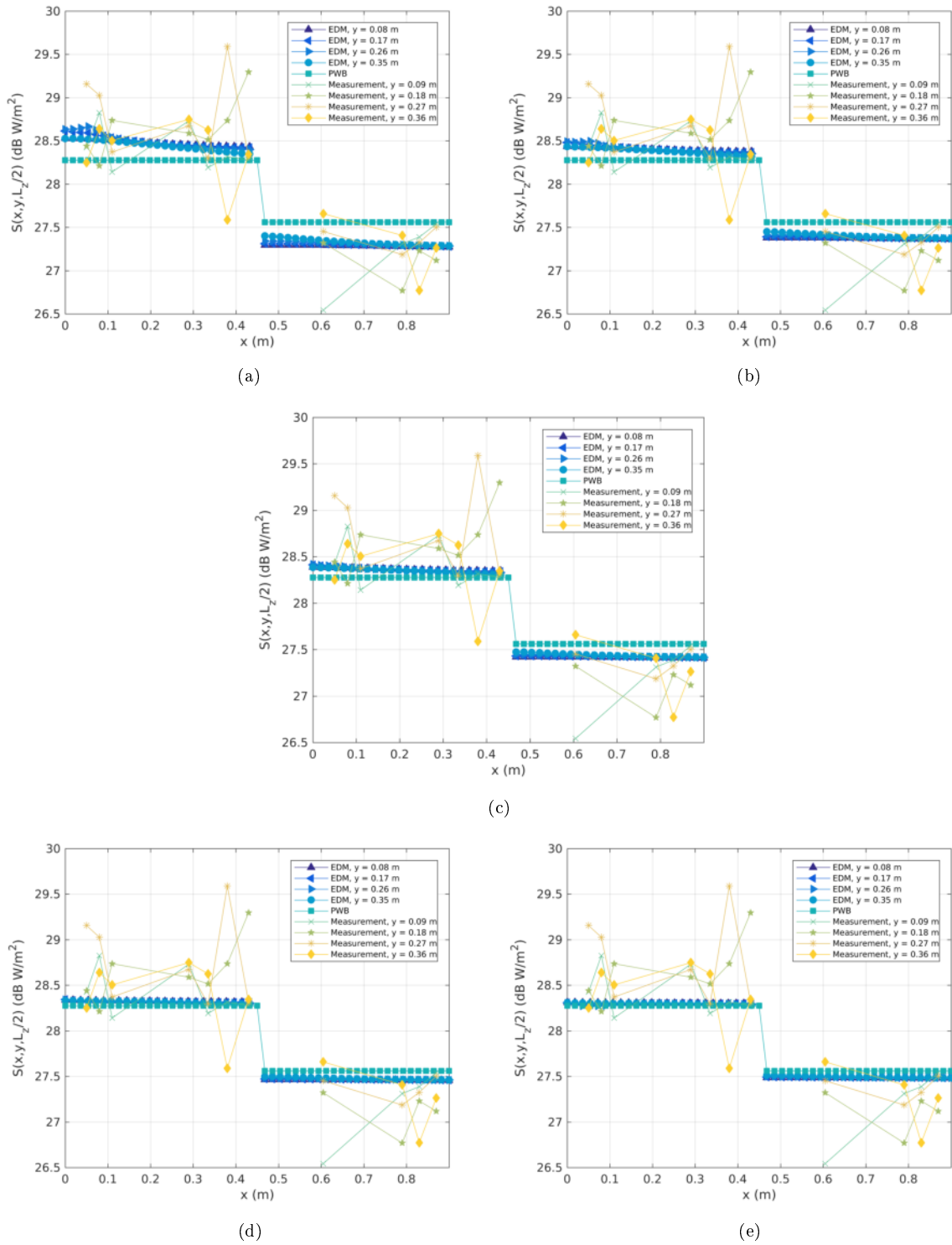
Figure 23: Power density profile in the x-direction along the cavity centre comparing the 3D EDM of the dual unloaded cavity and measurement (Flintoft et al., 2017): (a) $\kappa = 1/2$; (b) $\kappa = 3/4$; (c) $\kappa = 1$; (d) $\kappa = 3/2$; (e) $\kappa = 2$.
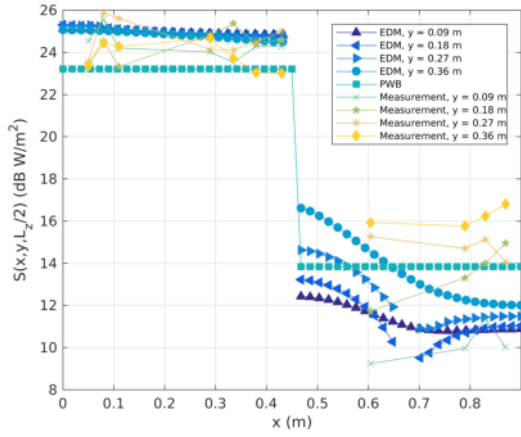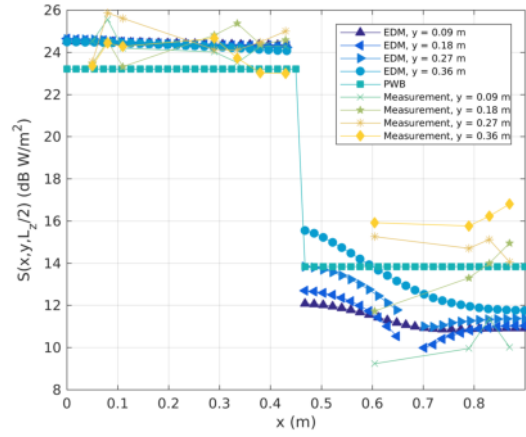
Figure 24: Power density profile in the x-direction along the cavity centre comparing the 3D EDM of the dual loaded cavity and measurement (Flintoft et al., 2017): (a) $\kappa = 1/2$; (b) $\kappa = 3/4$; (c) $\kappa = 1$; (d) $\kappa = 3/2$; (e) $\kappa = 2$.
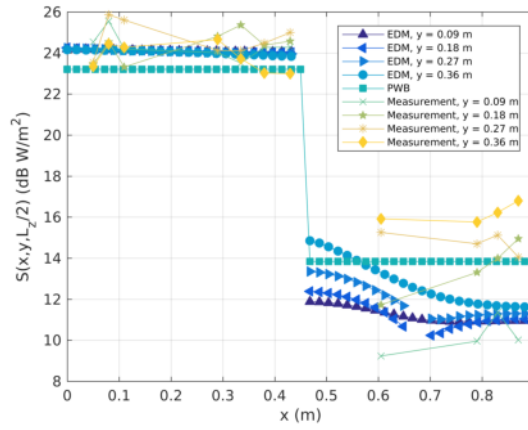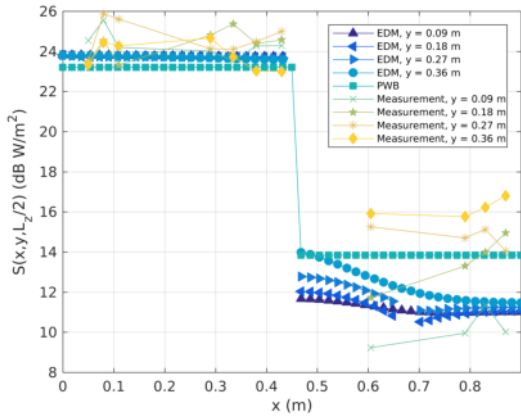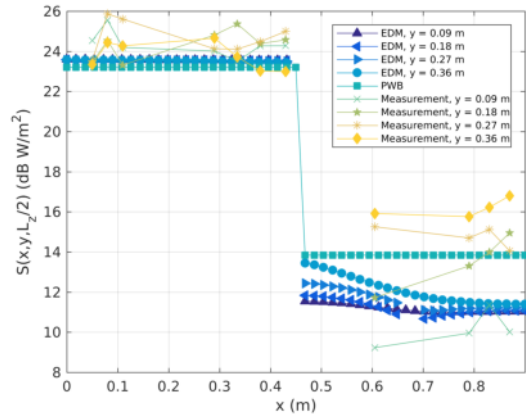
C. F. Eyring. Reverberation time in "dead rooms. *The Journal of the Acoustical Society of America*, 1 (2A):217–241, 1930. doi:10.1121/1.1915175.

I. D. Flintoft, A. C. Marvin, F. I. Funn, L. Dawson, X. Zhang, M. P. Robinson, and J. F. Dawson. Evaluation of the diffusion equation for modelling reverberant electromagnetic fields. *IEEE Transactions on Electromagnetic Compatibility*, 59(3):760–769, June 2017. doi:10.1109/TEMC.2016.2623356.

C. Foy, V. Valeau, A. Billon, J. Picaut, and A. Sakout. An empirical diffusion model for acoustic prediction in rooms with mixed diffuse and specular reflections. *Acta Acustica united with Acustica*, 95(1):97–105, 2009. doi:10.3813/aaa.918131.

C. Geuzaine and J.-F. Remacle. Gmsh: A 3-D finite element mesh generator with built-in pre- and post-processing facilities. *International Journal for Numerical Methods in Engineering*, 79(11):1309–1331, 2009. doi:10.1002/nme.2579.

F. Hecht. New development in freefem++. *Journal of Numerical Mathematics*, 20:251, 2013. doi:10.1515/jnum-2012-0013.

F. Hecht. *Freefem++*. Laboratoire Jacques-Louis Lions, Universit´e Pierre et Marie Curie, Paris, 3rd edition, May 2017, url: http://www.freefem.org/ff++/ftp/freefem++doc.pdf. For FreeFEM++ version 3.51.

Y. Jing and N. Xiang. On boundary conditions for the diffusion equation in room-acoustic prediction: Theory, simulations, and experiments. *The Journal of the Acoustical Society of America*, 123(1): 145–153, 2008. doi:10.1121/1.2805618.

L. V. Kantorovich and V. I. Krylov. *Approximate methods of higher analysis*. Interscience Publishers, New York, 3rd edition, 1964.

P.-L. Lions. On the Schwarz alternating method III: A variant for nonoverlapping subdomains. In *Third international symposium on domain decomposition methods for partial differential equations*, volume 6, pages 202–223. SIAM Philadelphia, PA, 1990.

J. M. Navarro and J. Escolano. Simulation of building indoor acoustics using an acoustic diffusion equation model. *Journal of Building Performance Simulation*, 8(1):3–14, 2015. doi:10.1080/19401493.2013.850534.

J. M. Navarro, J. Escolanoa, M. Cobos, and J. J. Lopez. Influence of the scattering and absorption coefficients on homogeneous room simulations that use a diffusion equation model. *J. Acoust. Soc. Am. 133 (3*, 133(3):1218–1221, Mar. 2013.

J. Picaut, L. Simon, and J.-D. Polack. Sound field in long rooms with diffusely reflecting boundaries. *Applied Acoustics*, 56(4):217 − 240, 1999. doi:10.1016/S0003-682X(98)00032-2.

W. C. Sabine. *Collected Papers on Acoustics*. Harvard University Press, 1922.

L. Savioja and U. P. Svensson. Overview of geometrical room acoustic modeling techniques. *The Journal of the Acoustical Society of America*, 138(2):708–730, 2015. doi:10.1121/1.4926438.

M. E. Sequeira and V. H. Cortínez. A simplified two-dimensional acoustic diffusion model for predicting sound levels in enclosures. *Applied Acoustics*, 73(8):842 − 848, 2012. doi:10.1016/j.apacoust.2012.02.012.

V. Valeau, J. Picaut, and M. Hodgson. On the use of a diffusion equation for room-acoustic prediction. *The Journal of the Acoustical Society of America*, 119(3):1504–1513, 2006. doi:10.1121/1.2161433.

V. Valeau, M. Hodgson, and J. Picaut. A diffusion-based analogy for the prediction of sound fields in fitted rooms. *Acta Acustica united with Acustica*, 93(1):94–105, 2007, url: http://www.ingentaconnect.com/content/dav/aaua/2007/00000093/00000001/art00011.

C. Visentin, N. Prodi, V. Valeau, and J. Picaut. A numerical investigation of the Fick's law of diffusion in room acoustics. *The Journal of the Acoustical Society of America*, 132(5):3180–3189, 2012. doi:10.1121/1.4756924.

C. Visentin, N. Prodi, V. Valeau, and J. Picaut. Experimental analysis of the relationship between reverberant acoustic intensity and energy density inside long rooms. *The Journal of the Acoustical Society of America*, 138(1):181–192, 2015. doi:10.1121/1.4922334.

N. Xiang, Y. Jing, and A. C. Bockman. Investigation of acoustically coupled enclosures using a diffusion-equation model. *The Journal of the Acoustical Society of America*, 126(3):1187–1198, 2009. doi:10.1121/1.3168507.

GNU Free Documentation License

Version 1.3, 3 November 2008
Copyright © 2000, 2001, 2002, 2007, 2008 Free Software Foundation, Inc.

`<https://fsf.org/>`

Everyone is permitted to copy and distribute verbatim copies of this license document, but changing it is not allowed.

Preamble

The purpose of this License is to make a manual, textbook, or other functional and useful document "free" in the sense of freedom: to assure everyone the effective freedom to copy and redistribute it, with or without modifying it, either commercially or noncommercially. Secondarily, this License preserves for the author and publisher a way to get credit for their work, while not being considered responsible for modifications made by others.

This License is a kind of "copyleft", which means that derivative works of the document must themselves be free in the same sense. It complements the GNU General Public License, which is a copyleft license designed for free software.

We have designed this License in order to use it for manuals for free software, because free software needs free documentation: a free program should come with manuals providing the same freedoms that the software does. But this License is not limited to software manuals; it can be used for any textual work, regardless of subject matter or whether it is published as a printed book. We recommend this License principally for works whose purpose is instruction or reference.

1. APPLICABILITY AND DEFINITIONS

This License applies to any manual or other work, in any medium, that contains a notice placed by the copyright holder saying it can be distributed under the terms of this License. Such a notice grants a world-wide, royalty-free license, unlimited in duration, to use that work under the conditions stated herein. The "**Document**", below, refers to any such manual or work. Any member of the public is a licensee, and is addressed as "**you**". You accept the license if you copy, modify or distribute the work in a way requiring permission under copyright law.

A "**Modified Version**" of the Document means any work containing the Document or a portion of it, either copied verbatim, or with modifications and/or translated into another language.

A "**Secondary Section**" is a named appendix or a front-matter section of the Document that deals exclusively with the relationship of the publishers or authors of the Document to the Document's overall subject (or to related matters) and contains nothing that could fall directly within that overall subject. (Thus, if the Document is in part a textbook of mathematics, a Secondary Section may not explain any mathematics.) The relationship could be a matter of historical connection with the subject or with related matters, or of legal, commercial, philosophical, ethical or political position regarding them.

The "**Invariant Sections**" are certain Secondary Sections whose titles are designated, as being those of Invariant Sections, in the notice that says that the Document is released under this License. If a section does not fit the above definition of Secondary then it is not allowed to be designated as Invariant. The Document may contain zero Invariant Sections. If the Document does not identify any Invariant Sections then there are none.

The "**Cover Texts**" are certain short passages of text that are listed, as Front-Cover Texts or Back-Cover Texts, in the notice that says that the Document is released under this License. A Front-Cover Text may be at most 5 words, and a Back-Cover Text may be at most 25 words.

A "**Transparent**" copy of the Document means a machine-readable copy, represented in a format whose specification is available to the general public, that is suitable for revising the document straightforwardly with generic text editors or (for images composed of pixels) generic paint programs or (for drawings) some widely available drawing editor, and that is suitable for input to text formatters or for automatic translation to a variety of formats suitable for input to text formatters. A copy made in an otherwise Transparent file format whose markup, or absence of markup, has been arranged to thwart or

discourage subsequent modification by readers is not Transparent. An image format is not Transparent if used for any substantial amount of text. A copy that is not "Transparent" is called "**Opaque**".

Examples of suitable formats for Transparent copies include plain ASCII without markup, Texinfo input format, LaTeX input format, SGML or XML using a publicly available DTD, and standard-conforming simple HTML, PostScript or PDF designed for human modification. Examples of transparent image formats include PNG, XCF and JPG. Opaque formats include proprietary formats that can be read and edited only by proprietary word processors, SGML or XML for which the DTD and/or processing tools are not generally available, and the machine-generated HTML, PostScript or PDF produced by some word processors for output purposes only.

The "**Title Page**" means, for a printed book, the title page itself, plus such following pages as are needed to hold, legibly, the material this License requires to appear in the title page. For works in formats which do not have any title page as such, "Title Page" means the text near the most prominent appearance of the work's title, preceding the beginning of the body of the text.

The "**publisher**" means any person or entity that distributes copies of the Document to the public.

A section "**Entitled XYZ**" means a named subunit of the Document whose title either is precisely XYZ or contains XYZ in parentheses following text that translates XYZ in another language. (Here XYZ stands for a specific section name mentioned below, such as "**Acknowledgements**", "**Dedications**", "**Endorsements**", or "**History**".) To "**Preserve the Title**" of such a section when you modify the Document means that it remains a section "Entitled XYZ" according to this definition.

The Document may include Warranty Disclaimers next to the notice which states that this License applies to the Document. These Warranty Disclaimers are considered to be included by reference in this License, but only as regards disclaiming warranties: any other implication that these Warranty Disclaimers may have is void and has no effect on the meaning of this License.

2. VERBATIM COPYING

You may copy and distribute the Document in any medium, either commercially or noncommercially, provided that this License, the copyright notices, and the license notice saying this License applies to the Document are reproduced in all copies, and that you add no other conditions whatsoever to those of this License. You may not use technical measures to obstruct or control the reading or further copying of the copies you make or distribute. However, you may accept compensation in exchange for copies. If you distribute a large enough number of copies you must also follow the conditions in section 3.

You may also lend copies, under the same conditions stated above, and you may publicly display copies.

3. COPYING IN QUANTITY

If you publish printed copies (or copies in media that commonly have printed covers) of the Document, numbering more than 100, and the Document's license notice requires Cover Texts, you must enclose the copies in covers that carry, clearly and legibly, all these Cover Texts: Front-Cover Texts on the front cover, and Back-Cover Texts on the back cover. Both covers must also clearly and legibly identify you as the publisher of these copies. The front cover must present the full title with all words of the title equally prominent and visible. You may add other material on the covers in addition. Copying with changes limited to the covers, as long as they preserve the title of the Document and satisfy these conditions, can be treated as verbatim copying in other respects.

If the required texts for either cover are too voluminous to fit legibly, you should put the first ones listed (as many as fit reasonably) on the actual cover, and continue the rest onto adjacent pages.

If you publish or distribute Opaque copies of the Document numbering more than 100, you must either include a machine-readable Transparent copy along with each Opaque copy, or state in or with each Opaque copy a computer-network location from which the general network-using public has access to download using public-standard network protocols a complete Transparent copy of the Document, free of added material. If you use the latter option, you must take reasonably prudent steps, when you begin distribution of Opaque copies in quantity, to ensure that this Transparent copy will remain thus accessible at the stated location until at least one year after the last time you distribute an Opaque copy (directly or through your agents or retailers) of that edition to the public.

It is requested, but not required, that you contact the authors of the Document well before redistributing any large number of copies, to give them a chance to provide you with an updated version of the Document.

4. MODIFICATIONS

You may copy and distribute a Modified Version of the Document under the conditions of sections 2 and 3 above, provided that you release the Modified Version under precisely this License, with the Modified Version filling the role of the Document, thus licensing distribution and modification of the Modified Version to whoever possesses a copy of it. In addition, you must do these things in the Modified Version:

A. Use in the Title Page (and on the covers, if any) a title distinct from that of the Document, and from those of previous versions (which should, if there were any, be listed in the History section of the Document). You may use the same title as a previous version if the original publisher of that version gives permission.

B. List on the Title Page, as authors, one or more persons or entities responsible for authorship of the modifications in the Modified Version, together with at least five of the principal authors of the Document (all of its principal authors, if it has fewer than five), unless they release you from this requirement.

C. State on the Title page the name of the publisher of the Modified Version, as the publisher.

D. Preserve all the copyright notices of the Document.

E. Add an appropriate copyright notice for your modifications adjacent to the other copyright notices.

F. Include, immediately after the copyright notices, a license notice giving the public permission to use the Modified Version under the terms of this License, in the form shown in the Addendum below.

G. Preserve in that license notice the full lists of Invariant Sections and required Cover Texts given in the Document's license notice.

H. Include an unaltered copy of this License.

I. Preserve the section Entitled "History", Preserve its Title, and add to it an item stating at least the title, year, new authors, and publisher of the Modified Version as given on the Title Page. If there is no section Entitled "History" in the Document, create one stating the title, year, authors, and publisher of the Document as given on its Title Page, then add an item describing the Modified Version as stated in the previous sentence.

J. Preserve the network location, if any, given in the Document for public access to a Transparent copy of the Document, and likewise the network locations given in the Document for previous versions it was based on. These may be placed in the "History" section. You may omit a network location for a work that was published at least four years before the Document itself, or if the original publisher of the version it refers to gives permission.

K. For any section Entitled "Acknowledgements" or "Dedications", Preserve the Title of the section, and preserve in the section all the substance and tone of each of the contributor acknowledgements and/or dedications given therein.

L. Preserve all the Invariant Sections of the Document, unaltered in their text and in their titles. Section numbers or the equivalent are not considered part of the section titles.

M. Delete any section Entitled "Endorsements". Such a section may not be included in the Modified Version.

N. Do not retitle any existing section to be Entitled "Endorsements" or to conflict in title with any Invariant Section.

O. Preserve any Warranty Disclaimers.

If the Modified Version includes new front-matter sections or appendices that qualify as Secondary Sections and contain no material copied from the Document, you may at your option designate some or all of these sections as invariant. To do this, add their titles to the list of Invariant Sections in the Modified Version's license notice. These titles must be distinct from any other section titles.

You may add a section Entitled "Endorsements", provided it contains nothing but endorsements of your Modified Version by various parties—for example, statements of peer review or that the text has been approved by an organization as the authoritative definition of a standard.

You may add a passage of up to five words as a Front-Cover Text, and a passage of up to 25 words as a Back-Cover Text, to the end of the list of Cover Texts in the Modified Version. Only one passage of Front-Cover Text and one of Back-Cover Text may be added by (or through arrangements made by) any one entity. If the Document already includes a cover text for the same cover, previously added by you or by arrangement made by the same entity you are acting on behalf of, you may not add another; but you may replace the old one, on explicit permission from the previous publisher that added the old one.

The author(s) and publisher(s) of the Document do not by this License give permission to use their names for publicity for or to assert or imply endorsement of any Modified Version.

5. COMBINING DOCUMENTS

You may combine the Document with other documents released under this License, under the terms defined in section 4 above for modified versions, provided that you include in the combination all of the Invariant Sections of all of the original documents, unmodified, and list them all as Invariant Sections of your combined work in its license notice, and that you preserve all their Warranty Disclaimers.

The combined work need only contain one copy of this License, and multiple identical Invariant Sections may be replaced with a single copy. If there are multiple Invariant Sections with the same name but different contents, make the title of each such section unique by adding at the end of it, in parentheses, the name of the original author or publisher of that section if known, or else a unique number. Make the same adjustment to the section titles in the list of Invariant Sections in the license notice of the combined work.

In the combination, you must combine any sections Entitled "History" in the various original documents, forming one section Entitled "History"; likewise combine any sections Entitled "Acknowledgements", and any sections Entitled "Dedications". You must delete all sections Entitled "Endorsements".

6. COLLECTIONS OF DOCUMENTS

You may make a collection consisting of the Document and other documents released under this License, and replace the individual copies of this License in the various documents with a single copy that is included in the collection, provided that you follow the rules of this License for verbatim copying of each of the documents in all other respects.

You may extract a single document from such a collection, and distribute it individually under this License, provided you insert a copy of this License into the extracted document, and follow this License in all other respects regarding verbatim copying of that document.

7. AGGREGATION WITH INDEPENDENT WORKS

A compilation of the Document or its derivatives with other separate and independent documents or works, in or on a volume of a storage or distribution medium, is called an "aggregate" if the copyright resulting from the compilation is not used to limit the legal rights of the compilation's users beyond what the individual works permit. When the Document is included in an aggregate, this License does not apply to the other works in the aggregate which are not themselves derivative works of the Document.

If the Cover Text requirement of section 3 is applicable to these copies of the Document, then if the Document is less than one half of the entire aggregate, the Document's Cover Texts may be placed on covers that bracket the Document within the aggregate, or the electronic equivalent of covers if the Document is in electronic form. Otherwise they must appear on printed covers that bracket the whole aggregate.

8. TRANSLATION

Translation is considered a kind of modification, so you may distribute translations of the Document under the terms of section 4. Replacing Invariant Sections with translations requires special permission from their copyright holders, but you may include translations of some or all Invariant Sections in addition to the original versions of these Invariant Sections. You may include a translation of this License, and all the license notices in the Document, and any Warranty Disclaimers, provided that you also include the original English version of this License and the original versions of those notices and disclaimers. In case of a disagreement between the translation and the original version of this License or a notice or disclaimer, the original version will prevail.

If a section in the Document is Entitled "Acknowledgements", "Dedications", or "History", the requirement (section 4) to Preserve its Title (section 1) will typically require changing the actual title.

9. TERMINATION

You may not copy, modify, sublicense, or distribute the Document except as expressly provided under this License. Any attempt otherwise to copy, modify, sublicense, or distribute it is void, and will automatically terminate your rights under this License.

However, if you cease all violation of this License, then your license from a particular copyright holder is reinstated (a) provisionally, unless and until the copyright holder explicitly and finally terminates your license, and (b) permanently, if the copyright holder fails to notify you of the violation by some reasonable means prior to 60 days after the cessation.

Moreover, your license from a particular copyright holder is reinstated permanently if the copyright holder notifies you of the violation by some reasonable means, this is the first time you have received notice of violation of this License (for any work) from that copyright holder, and you cure the violation prior to 30 days after your receipt of the notice.

Termination of your rights under this section does not terminate the licenses of parties who have received copies or rights from you under this License. If your rights have been terminated and not permanently reinstated, receipt of a copy of some or all of the same material does not give you any rights to use it.

10. FUTURE REVISIONS OF THIS LICENSE

The Free Software Foundation may publish new, revised versions of the GNU Free Documentation License from time to time. Such new versions will be similar in spirit to the present version, but may differ in detail to address new problems or concerns. See https://www.gnu.org/licenses/.

Each version of the License is given a distinguishing version number. If the Document specifies that a particular numbered version of this License "or any later version" applies to it, you have the option of following the terms and conditions either of that specified version or of any later version that has been published (not as a draft) by the Free Software Foundation. If the Document does not specify a version number of this License, you may choose any version ever published (not as a draft) by the Free Software Foundation. If the Document specifies that a proxy can decide which future versions of this License can be used, that proxy's public statement of acceptance of a version permanently authorizes you to choose that version for the Document.

11. RELICENSING

"Massive Multiauthor Collaboration Site" (or "MMC Site") means any World Wide Web server that publishes copyrightable works and also provides prominent facilities for anybody to edit those works. A public wiki that anybody can edit is an example of such a server. A "Massive Multiauthor Collaboration" (or "MMC") contained in the site means any set of copyrightable works thus published on the MMC site.

"CC-BY-SA" means the Creative Commons Attribution-Share Alike 3.0 license published by Creative Commons Corporation, a not-for-profit corporation with a principal place of business in San Francisco, California, as well as future copyleft versions of that license published by that same organization.

"Incorporate" means to publish or republish a Document, in whole or in part, as part of another Document.

An MMC is "eligible for relicensing" if it is licensed under this License, and if all works that were first published under this License somewhere other than this MMC, and subsequently incorporated in whole or in part into the MMC, (1) had no cover texts or invariant sections, and (2) were thus incorporated prior to November 1, 2008.

The operator of an MMC Site may republish an MMC contained in the site under CC-BY-SA on the same site at any time before August 1, 2009, provided the MMC is eligible for relicensing.